





Calcium-dependent protein kinase 29 modulates PIN-FORMED polarity and *Arabidopsis* development via its own phosphorylation code

Hyodong Lee ¹, Anindya Ganguly ^{1,†}, Song Baik ¹ and Hyung-Taeg Cho ^{1,*‡}

¹ Department of Biological Sciences, Seoul National University, Seoul 08826, Korea

*Author for correspondence: htcho@snu.ac.kr

[†]Present address: Molecular Physiology and Biological Physics, University of Virginia, VA 22903, USA

[‡]Senior author.

H.L. performed most experiments, A.G. conducted the initial experiment to screen PIN-interacting proteins, and S.B. contributed to *in vivo* protein phosphorylation analysis; H.L., A.G., and H.-T.C. designed the study, analyzed the data, and wrote the manuscript.

The author responsible for distribution of materials integral to the findings presented in this article in accordance with the policy described in the Instructions for Authors (<https://academic.oup.com/plcell>) is: Hyung-Taeg Cho (htcho@snu.ac.kr).

Abstract

PIN-FORMED (PIN)-mediated polar auxin transport (PAT) is involved in key developmental processes in plants. Various internal and external cues influence plant development via the modulation of intracellular PIN polarity and, thus, the direction of PAT, but the mechanisms underlying these processes remain largely unknown. PIN proteins harbor a hydrophilic loop (HL) that has important regulatory functions; here, we used the HL as bait in protein pulldown screening for modulators of intracellular PIN trafficking in *Arabidopsis thaliana*. Calcium-dependent protein kinase 29 (CPK29), a Ca^{2+} -dependent protein kinase, was identified and shown to phosphorylate specific target residues on the PIN-HL that were not phosphorylated by other kinases. Furthermore, loss of CPK29 or mutations of the phospho-target residues in PIN-HLs significantly compromised intracellular PIN trafficking and polarity, causing defects in PIN-mediated auxin redistribution and biological processes such as lateral root formation, root twisting, hypocotyl gravitropism, phyllotaxis, and reproductive development. These findings indicate that CPK29 directly interprets Ca^{2+} signals from internal and external triggers, resulting in the modulation of PIN trafficking and auxin responses.

Introduction

Auxin acts as a morphogen, influencing a wide range of fundamental processes in plant growth and development. Morphogenic local auxin gradients are established mainly by polar auxin transport (PAT), which is driven by asymmetrically localized auxin transporters in the plasma membrane (PM). PIN-FORMED (PIN) auxin efflux carriers show conspicuous polar localizations in the PM and act as key mediators for PAT (Kleine-Vehn and Friml, 2008). PIN proteins consist of a central hydrophilic loop (HL; ~50 to ~300 residues)

flanked on either side by five transmembrane helices (Křeček et al., 2009; Ganguly, Sasayama, et al., 2012). Long-HL PINs (HL approximately > 300 residues) display a characteristic asymmetric distribution pattern (i.e. polarity) depending on PIN species, developmental stage, and cell type, and also exhibit polarity changes in response to environmental stimuli such as light and gravity (Friml et al., 2002; Wiśniewska et al., 2006; Kleine-Vehn et al., 2010; Ding et al., 2011). Developmental and environmental dynamics of PIN polarity are accomplished by the modulation of

intracellular PIN trafficking, for which post-translational modifications of the HL domain, such as phosphorylation and ubiquitylation, are instrumental (Leitner et al., 2012; Ganguly et al., 2014; Barbosa et al., 2018).

Phosphorylation of PIN-HLs has been implicated in the modulation of PIN polarity for maintenance or flickering of local auxin gradients and also in the regulation of PIN activity. At least three families of protein kinases have been identified that phosphorylate PIN-HLs: AGC-type protein kinases (PINOID [PID], WAGs, D6 protein kinases [D6PKs], and AGC1-12), mitogen-activated protein kinases, and a calcium-dependent protein kinase (CPK)-related kinase (CRK5) (as reviewed by Armengot et al., 2016; Barbosa et al., 2018; Hammes et al., 2021). Among these kinases, AGC-type kinases appear to play major roles in PIN trafficking and activity. Consequently, AGC-type kinases are the most comprehensively characterized and their individual phosphorylation target sites in the PIN-HLs are well known (Zourelidou et al., 2009, 2014; Dhonukshe et al., 2010; Huang et al., 2010; Ganguly, Lee, et al., 2012; Barbosa et al., 2014; Haga et al., 2018). Nevertheless, since auxin responses, including PIN-mediated regulation of auxin distribution, are influenced by a wide range of internal and external signals, the regulatory cues in the PIN-HL and their trans-acting factors are therefore likely to be more diverse than those identified to date. To address these questions, we searched for PIN-HL-interacting proteins and identified and characterized CPK29 as a previously unknown modulator for PIN trafficking, most likely via sensing Ca^{2+} signals.

Ca^{2+} serves as a universal signaling messenger for various internal and external developmental cues. Stimulus-induced changes in cytosolic Ca^{2+} concentration are interpreted by Ca^{2+} -binding proteins, which then target diverse Ca^{2+} -responder proteins such as enzymes, transporters, and transcriptional regulators (Dodd et al., 2010; Valmonte et al., 2014). Among the Ca^{2+} -binding proteins, CPKs are unique in that they act not only as Ca^{2+} readers but also as responders (Valmonte et al., 2014). CPKs phosphorylate a wide spectrum of proteins such as metabolic enzymes, signaling proteins, membrane transporters, and transcription factors, and mediate biological processes including cellular signaling, gene regulation, ion currency, hormone biosynthesis, biotic/abiotic responses, guard cell movement, tip growth, and organ development (Delormel and Boudsocq, 2019).

Ca^{2+} was previously implicated in PAT (Dela Fuente and Leopold, 1973), and several lines of evidence suggested links between Ca^{2+} signaling and the modulation of PIN trafficking. Two Ca^{2+} -binding proteins, PID-BINDING PROTEIN 1 (PBP1) and TOUCH 3 (TCH3), were shown to activate PID, implying that Ca^{2+} might work through PID to affect PIN trafficking (Benjamins et al., 2003). Inositol triphosphate-induced Ca^{2+} -signaling was shown to be involved in the modulation of PIN polarity (Zhang et al., 2011). Additionally, CRK5 was shown to modulate PIN2 trafficking and polarity and to phosphorylate PIN2-HL, though the phosphorylation sites were not identified (Rigó et al., 2013). CRK5 is one of

the eight Arabidopsis CRKs that form a sister group with CPKs (Delormel and Boudsocq, 2019). CRKs, unlike CPKs, are not able to directly bind Ca^{2+} due to degeneration of their EF-hands, but some can be activated by Ca^{2+} -bound calmodulin (Wang et al., 2004; Popescu et al., 2007). Although these previous studies demonstrated the involvement of Ca^{2+} in PAT, most likely via modulation of PIN trafficking, the direct mechanistic component that Ca^{2+} acts upon and the underlying mechanisms responsible for its modulation of PIN trafficking have remained to be characterized. Our study demonstrates that CPK29 directly phosphorylates the unique residues of the HL of major long PINs, and that these CPK29-target phosphorylation sites are involved in modulation of the recycling pathway of PINs and diverse PIN-mediated developmental processes.

Results

CPK29 phosphorylates PIN-HLs

CPK29 was initially identified by protein pull-down screening of a protein extract from Arabidopsis seedlings with bacterially expressed PIN2-HL as bait as described in “Materials and Methods”. In *in vitro* pull-down assays with bacterium-expressed CPK29 and PIN-HLs, CPK29 interacted not only with PIN2-HL but also with HLs from PIN1 and PIN3 (Figure 1A).

In vitro phosphorylation analysis showed that CPK29 underwent autophosphorylation and directly phosphorylated the HLs of PIN1, PIN2, and PIN3, and also showed that phosphorylation activity was enhanced by Ca^{2+} (Figure 1B; Supplemental Figure S1). CPK29 contains four Ca^{2+} -binding EF hands at the C-terminal region (Supplemental Figure S2A). Phosphorylated CPK29 and PIN-HLs were analyzed by mass spectrometry to identify the phosphorylated residues. One Ser residue (S446) of CPK29 and multiple Ser/Thr residues of PIN-HLs were identified as phosphorylated (Supplemental Table S1). The phosphorylation sites were confirmed by *in vitro* phosphorylation assays of mutated proteins lacking phosphorylation residues. Among the phosphorylated residues identified by mass spectrometry, testable residues were selected from redundantly represented peptides (Supplemental Table S1). Unexpectedly, the phosphodeficient S446A mutation of CPK29 enhanced CPK29 autophosphorylation and CPK29-mediated phosphorylation of PIN-HLs (Figure 1C; Supplemental Figure S1), indicating that residues other than S446 could be autophosphorylated in CPK29, and that S446 autophosphorylation was inhibitory or modulatory for the instigation of the phosphorylation cascade. Consistent with this idea, several CPK homologs from bean and tobacco plants similarly show autophosphorylation that is inhibitory to their kinase activities (Saha and Singh, 1995; Ito et al., 2017).

In PIN1, the S253A mutation almost completely eliminated the CPK29-mediated phosphorylation capacity of the HL (Figure 1D), and the S259A mutation in PIN2-HL also greatly hampered its phosphorylation by CPK29 (Figure 1E). These phosphorylatable Ser residues in PIN1 and PIN2 reside

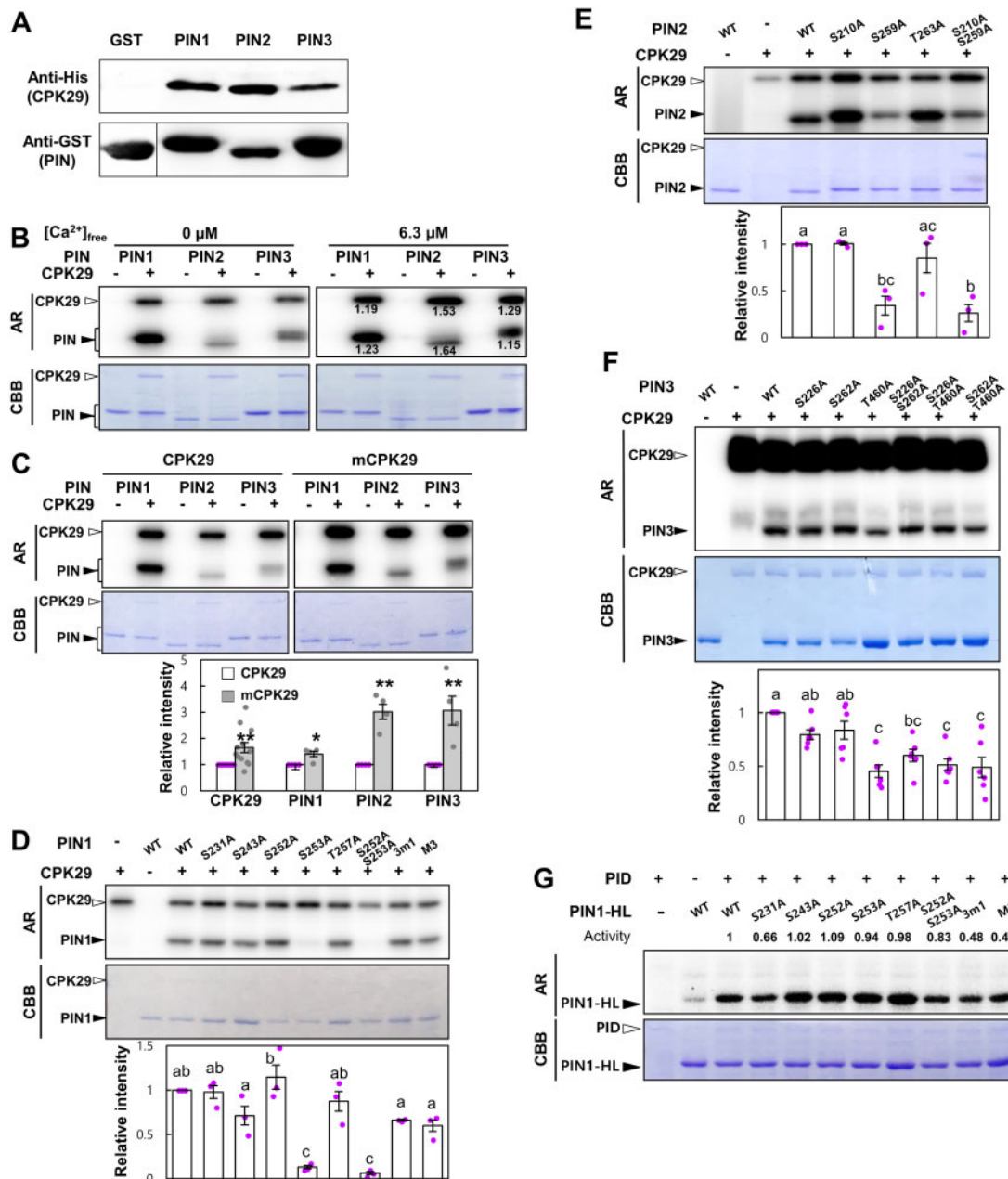


Figure 1 CPK29 directly interacts with and phosphorylates PIN-HLs. *A*, *In vitro* pull-down assay of interaction between CPK29 and PIN-HLs. GST or the indicated GST:PIN fusion proteins were used as preys to pull-down His:CPK29. *B*, Effect of Ca²⁺ on CPK29-mediated *in vitro* phosphorylation of PIN-HLs. Numbers below the autoradiogram (AR) bands represent phosphorylation intensities with 6.3 μM Ca²⁺ relative to the corresponding intensities with 0 μM Ca²⁺. *C*, Effect of a site mutation (S446A) of CPK29 (mCPK29) on its autophosphorylation and phosphorylation of PIN-HLs *in vitro*. Relative intensity data represent means ± se (standard error) of the relative AR band intensities of CPK29 and PINs (*n* = 12 for CPK29 and *n* = 4 for PINs; significantly different from the CPK29 value, **P* < 0.05; ***P* < 0.01, Student's *t* test). *D–F*, *In vitro* phosphorylation assays of phospho-mutated PIN-HLs with CPK29 (*D*, PIN1-HL; *E*, PIN2-HL; *F*, PIN3-HL). phospho-mutations of PIN1 at sites 3 ml (S209/212/215A) and M3 (3 ml + T227/S231A) *D*, were as described in Supplemental Figure S11. Relative intensity data represent means ± se of the relative AR band intensities of PINs (*n* = 3 in *D* and *E* and 6 in *F*). Kinase activities as indicated by relative AR band intensity in panels (*B–F*) were normalized with the CBB band intensity. Different letters in the graphs denote significant differences (*D–F*; ANOVA test, *P* < 0.05). 'n' in panels (*C–F*) denotes the number of independent assays. *G*, *In vitro* phosphorylation assays of phospho-mutated PIN-HLs with PID, an AGC protein kinase. Activities were normalized by CBB band intensity.

at the same conserved position in orthologous sequences of the two PINs (Supplemental Figure S3A). Although this phospho-Ser is found in the immediate next of a 'TPRXS' (X is any amino acid) motif targeted by AGC-type protein

kinases (Dhonukshe et al., 2010; Huang et al., 2010; Zourelidou et al., 2014; Haga et al., 2018; Supplemental Figure S4A), its unique and conserved position prompt us to hypothesize that this Ser in both PIN1 and PIN2 has long

been specifically targeted by CPK29 since their ancestral protein. Conversely, this Ser position is not conserved in the PIN3, PIN4, and PIN7 clusters (Supplemental Figure S3A), indicative of their divergent modulatory mechanism from that of PIN1 and PIN2. Mutagenesis analysis showed that PIN3-HL had at least one major CPK29-target residue (T460), whose phospho-defective mutation significantly compromised CPK29-mediated *in vitro* phosphorylation (Figure 1F). T460 does not appear to be conserved among PIN3 orthologs and close paralogs (Supplemental Figure S3B). S226 and S262 of PIN3 also could be minor targets of CPK29: their single mutations were not effective but the double mutations of both residues somewhat interfered with PIN3-HL phosphorylation (Figure 1F). Phospho-mutated PIN2-HL and PIN3-HL both retained residual phosphorylation, indicating the presence of additional CPK29-target residues in PIN2 and PIN3, in contrast to the dominant target S253 in PIN1.

The *in vitro* CPK29-phosphorylation target residues in PIN-HLs and CPK29 described above were also identified in the phosphopeptide-enriched fractions from Arabidopsis plants by our mass spectrometry analysis and by other previous studies (Supplemental Table S2), indicating that those residues are also phosphorylated *in vivo*.

The specificity of CPK29 in selecting phosphorylation targets was investigated further by testing phosphorylation sites typically targeted by AGC-type kinases, namely '3m1' (S209/212/215A) and 'M3' (3m1 + T227/S231A) sites (Ganguly, Lee, et al., 2012; Sasayama et al., 2013; Ki et al., 2016). Mutation of these sites did not significantly affect CPK29-mediated phosphorylation of PIN1-HL (Figure 1D). Moreover, mutation of S231 and S252 of PIN1, which are located in two of the three TPRXS motifs targeted by AGC kinases (Supplemental Figure S4A), did not affect CPK29-mediated PIN1 phosphorylation (Figure 1D). Similarly, the mutation of CPK29-target residues did not considerably hinder PINOID (PID, a representative AGC-type protein kinase modulating PIN trafficking)-mediated phosphorylation of PIN1-HL, whereas PID activity was impacted by mutation of the 3 m1 and M3 phosphorylation sites (Figure 1G). Together, these results suggest that PID and CPK29 have distinct preferences for phospho-targets in the PIN-HL.

CPK29 harboring a phospho-defective S446A mutation (mCPK29) retained the capacity for autophosphorylation and exhibited enhanced PIN phosphorylation. Next, therefore, we sought additional phosphorylation sites in CPK29 and investigated whether wild-type (WT) CPK29 and mCPK29 gave different phosphorylation profiles with regard to the specificities of their target residues. Mass spectrometry analysis revealed additional phosphorylation sites targeted by mCPK29 in both CPK29 and PIN-HLs (Supplemental Table S3; Supplemental Figure S4). Whereas S446 was located in the calmodulin-like domain and conserved among orthologs and close paralogs of CPK29, additional autophosphorylation sites were found throughout the CPK29 protein (Supplemental Figures S4B and S5 and Supplemental Data Set 1). Although some phosphorylation

targets were common to both WT CPK29 and mCPK29, some distinct target preferences were observed for the WT and mutated CPK29 proteins (Supplemental Figure S4A). It is conceivable that S446 in CPK29 and closely related CPKs might play a unique role in the modulation of the kinase activity.

CPK29 localizes to the PM

CPK29 is ubiquitously expressed in seedling organs, mature leaves, and floral organs, with high expression levels observed in vascular tissues (Supplemental Figure S6). The CPK29 protein was predominantly detected in the membrane fraction of total protein extracts from seedlings but not in the cytosolic fraction as was PIN1 (Figure 2A). In leaf mesophyll cell protoplasts, the CPK29 protein was co-localized with the PM (Figure 2B). In its expressing cell types such as hypocotyl epidermis, root vasculature, lateral root (LR) primordia, and root epidermis, the CPK29:GFP (green fluorescence protein) fusion protein, which was expressed under its own promoter (*ProCPK29:CPK29:GFP*), was mainly localized to the PM (Supplemental Figure S6, F, G, I, J, and K). The CPK29-GFP accumulation in the root epidermis of *ProCPK29:CPK29:GFP* transformants was low but obvious when compared with the nontransgenic WT tissue (Supplemental Figure S6, K and S6, L), consistently with the previous study reporting a low transcriptional expression of CPK29 in the root epidermis (Brady et al., 2007). Unlike PIN2, CPK29 does not appear to readily pass through the lytic pathway, as demonstrated by limited vacuolar accumulation of CPK29 under dark treatment in the root epidermis (Figure 2C). On the other hand, both CPK29 and PIN3 stably resided at the PM after dark treatment in the hypocotyl epidermis (Supplemental Figure S7A), implying that the dark-inducible lytic pathway is dependent on tissue and/or protein types. PINs and D6PK, an AGC-type protein kinase that phosphorylates PINs, are actively recycled between the PM and endosomes (Geldner et al., 2001; Barbosa et al., 2014). This can be observed using brefeldin A (BFA, an exocytic vesicle-trafficking blocker), which induces the internal accumulation of the recycling proteins. However, internal compartmentalization of the CPK29 signal was very limited with BFA treatment in the epidermal cells of root and hypocotyl, whereas PIN2 and PIN3 were internalized (Figure 2D; Supplemental Figure S7B), indicating that PM-localized CPK29 did not actively recycle.

When CPK29:RFP was co-expressed with PIN2:GFP, the two fusion proteins co-localized at the PM (Supplemental Figure S7C). To examine the *in vivo* interaction between CPK29 and PIN2, Förster resonance energy transfer by fluorescence lifetime imaging (FRET-FLIM) analysis was conducted with transgenic plants expressing both CPK29:RFP and PIN2:GFP. The fluorescence lifetime of PIN2:GFP was significantly decreased in the CPK29:RFP/PIN2:GFP double transgenic plant compared to the PIN2:GFP single transgenic plant (Figure 2, E and F), indicating that the resonance energy from PIN2:GFP was transferred to CPK29:RFP by the physical interaction between two proteins *in vivo*.

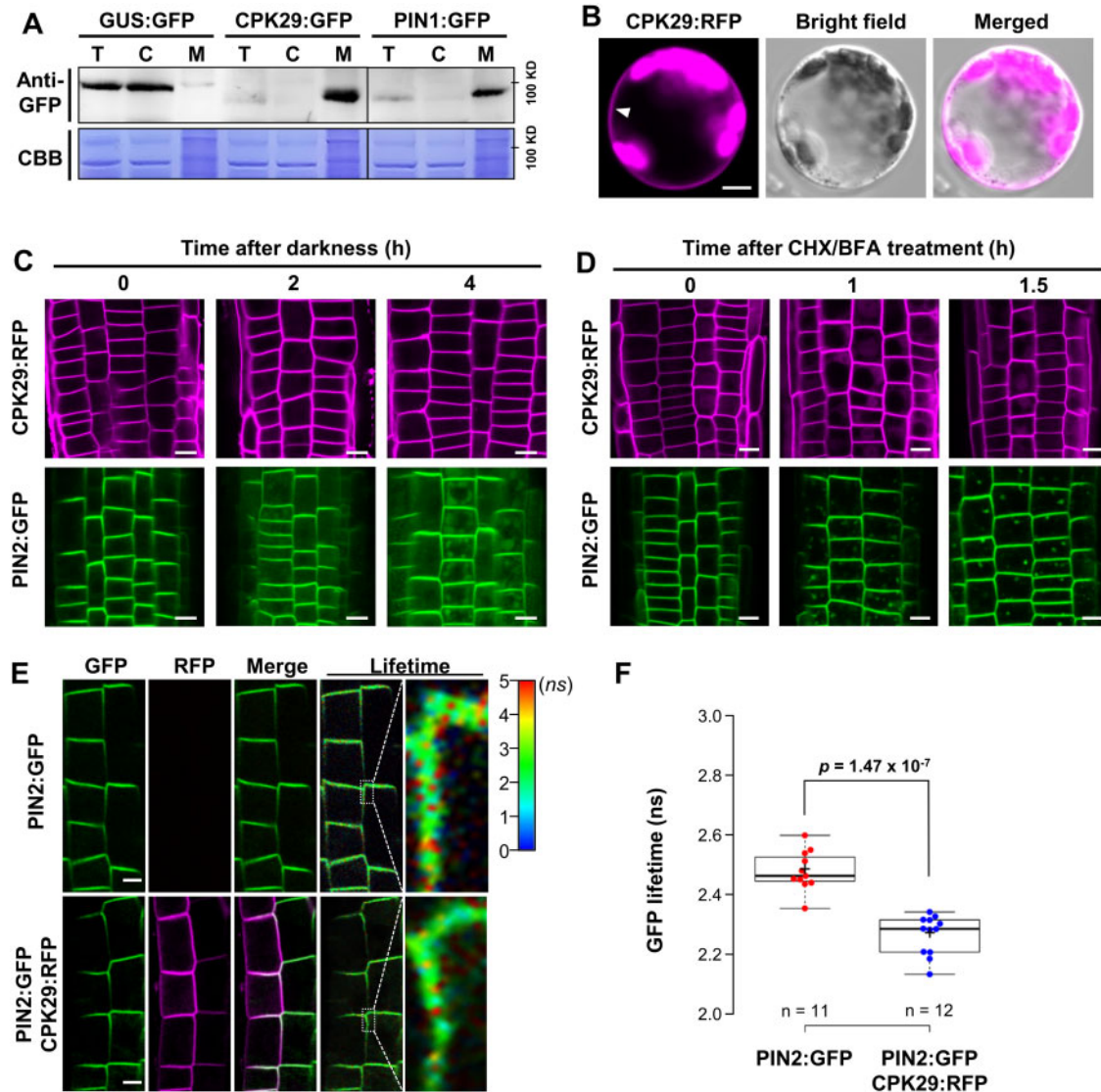


Figure 2 CPK29 localizes to the PM and interacts with PIN2 *in vivo*. A, CPK29 is detected predominantly in the membrane fraction. GUS:GFP and CPK29:GFP were expressed under *ProCPK29*, and PIN1:GFP under *ProPIN1*. T, C, and M denote total protein, cytosolic fraction, and membrane fraction, respectively. An equivalent gel shown by CBB staining was used for immunoblotting. B, PM localization (arrowhead) of CPK29 (*Pro35S:CPK29:RFP*) in the Arabidopsis leaf mesophyll protoplast. C, Effect of dark treatment on the stability of CPK29 (*Pro35S:CPK29:RFP*) and PIN2 (*ProPIN2:PIN2:GFP*) in the PM of the root epidermal cell. D, Effect of BFA on the recycling of CPK29 and PIN2 between the PM and endosomes in the root epidermal cell. Seedling roots were pretreated with CHX (50 μ M) for 30 min and treated with BFA (25 μ M) together with CHX (50 μ M) for given time. E and F, FRET-FLIM analysis for the *in vivo* interaction between PIN2 and CPK29 in the root epidermal cell. The *ProPIN2:PIN2:GFP* transformant and the double transformant with *ProPIN2:PIN2:GFP* and *Pro35S:CPK29:RFP* were compared to quantitatively estimate the GFP life time in the FRET-FLIM analysis. Color scale in (E) indicates GFP lifetime in nanosecond (ns). Bar = 5 (B) and 10 μ m (C–E). ‘n’ denotes the number of independent observations (F).

CPK29 is required for the intracellular polarity and trafficking of PINs

CPK29-mediated direct phosphorylation of specific residues in PINs suggests that these residues could be involved in intracellular trafficking of PINs since PIN phosphorylation is modulatory for PIN trafficking. To test this hypothesis, phospho-mutant versions of PINs were generated for the CPK29-target residues, and their intracellular trafficking behavior was examined. Significant defects in PIN intracellular trafficking and polarity were observed upon the loss of CPK29 (*cpk29-2*), including the

decreased basal polarity of PIN1 and apical polarity of PIN2, and increased internal accumulation of PIN proteins (Figure 3, A–D). Phospho-defective mutation of the CPK29-target residues, that is, S253A in PIN1 and S259A in PIN2, generated similar results to those seen with the *cpk29* mutant (Figure 3, A–D). In contrast, phospho-mimetic mutations of the target residues (S253D/E in PIN1 and S259D/E in PIN2) gave rise to modest decreases in polarity but did not cause significant intracellular accumulation of the PIN proteins (Figure 3, A–D).

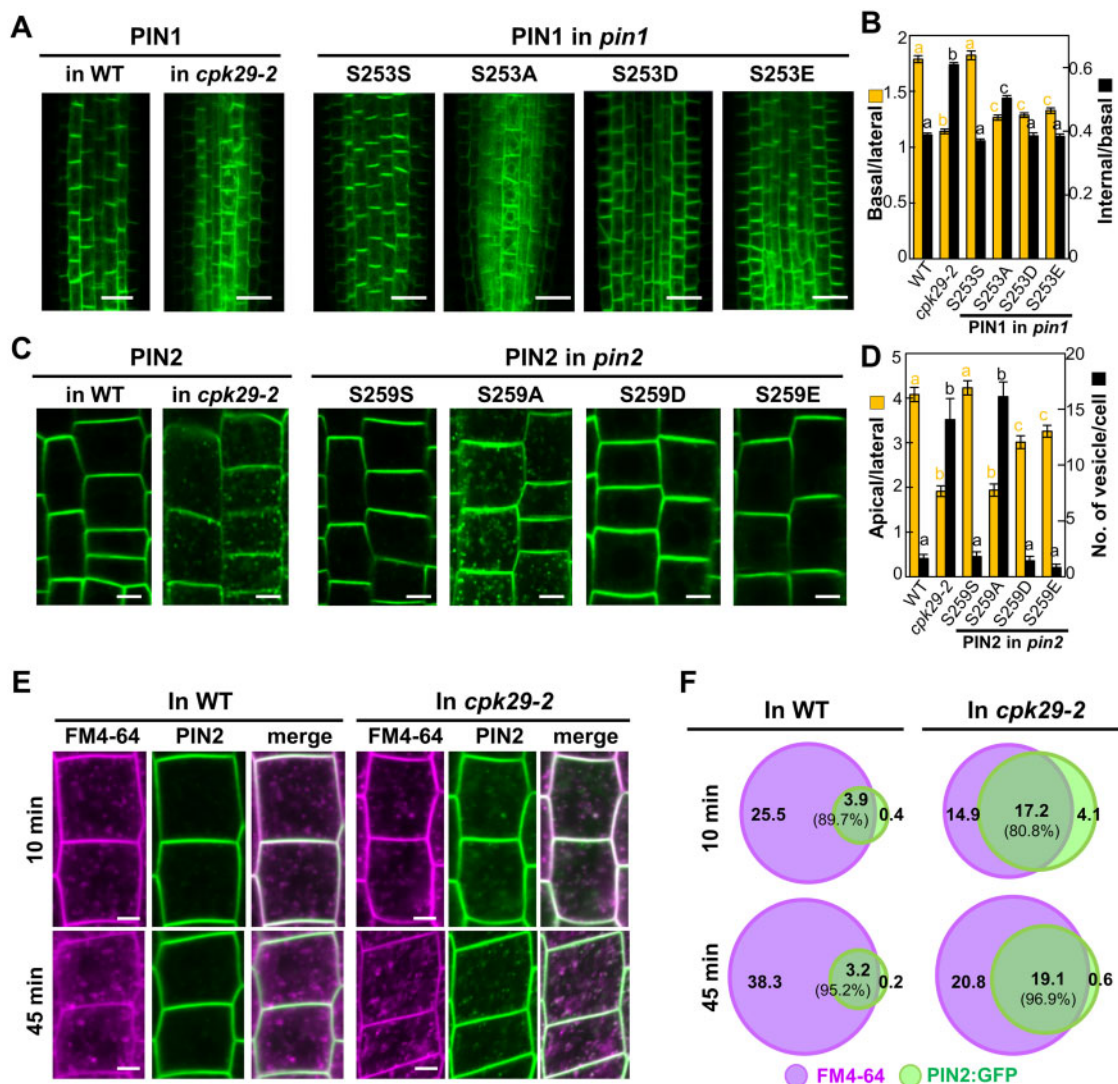


Figure 3 CPK29 and CPK29-target residues in PIN-HLs are necessary for normal intracellular trafficking of PINs. A and C, Subcellular localization of PINs (*ProPIN:PIN:GFP*) in the root vasculature (A for PIN1) and epidermis (C for PIN2). WT PIN was introduced into WT and *cpk29-2* mutant plants, and phospho-mutated versions of PINs were introduced into the *pin* mutants. Bar = 20 (A) and 5 μ m (C). B and D, Quantification of PIN polarity or trafficking parameters (B, basal versus lateral and internal versus basal PIN1 intensity; D, apical versus lateral PIN2 intensity and number of vesicles containing PIN2) shown in panels A and C, respectively. Data represent means \pm SE ($n = 186$ –268 cells of 10–21 roots [B] and 33–112 cells of 6–15 roots [D] from at least three independent transgenic lines for each construct). Different letters denote significant differences (ANOVA test, $P < 0.05$). E and F, The co-localization dynamics between FM4–64- and PIN2 (*ProPIN2:PIN2:GFP*)-containing intracellular vesicles after FM4–64 treatment (time indicated in the left) in the root epidermis of WT and *cpk29-2* mutant. Bar = 5 μ m (E). The values in Venn diagrams (F) denote the average numbers (per cell) of only FM4–64-including vesicles (red), only PIN2-including vesicles (green), or co-localized vesicles including both signals (overlapped). Percentage values inside parentheses indicate the ratio of co-localized vesicle number among PIN2 vesicles.

To learn which trafficking vesicles PIN proteins localize upon the loss of CPK29, co-localization of PIN2:GFP with the fluorescent endocytic tracer FM4–64 was examined. Exogenously applied FM4–64 immediately incorporates into the PM and undergoes an endocytic process that delivers the invaginated vesicles all the way to the vacuole via early/late endosomes or back to the PM via early endosomes (Reyes et al., 2011). FM4–64 reaches early endosomes within 5 min and the vacuole in 2 h after application (Grebe et al., 2003; Dettmer et al., 2006; Kleine-Vehn et al., 2008). We examined the co-localization at two time points, 10 and 45

min after FM4–64 application during which FM4–64 stays at endosomes, with the *ProPIN2:PIN2:GFP* transformant in WT or *cpk29-2* mutant background (Figure 3, E and F). The number of endocytosed FM4–64 vesicles increased over time. At both time points, the majority of internalized PIN2 vesicles in the *cpk29-2* mutant overlapped with the FM4–64 vesicles; $\sim 81\%$ at 10 min and $\sim 97\%$ at 45 min. Although the number of internalized PIN2 vesicles in WT was much smaller than in *cpk29-2*, they also mostly co-localized with the FM4–64 vesicles. Similar results were obtained with phospho-defective (S269A) PIN2 (Supplemental Figure S8).

This co-localization data suggest that the internalized PIN2 protein in the *cpk29-2* mutant cells is localized mostly likely to the early endosomes and that CPK29 affects the PIN trafficking with regard to endosomal-trafficking dynamics.

BFA-induced internal accumulation of PM-targeting proteins, under the inhibition of their *de novo* synthesis, is a useful tool for estimating the rate of protein recycling between the PM and endosomes (Geldner et al., 2001; Barbosa et al., 2014). The BFA-induced intracellular trafficking kinetics of PIN1 and PIN2 were examined in WT and *cpk29-2* mutant plants, and with phospho-defective and -mimetic versions of PIN1 and PIN2 (Figure 4, A–D; Supplemental Figure S9). In the presence of BFA, internal accumulation of PIN1 and PIN2 occurred more rapidly in the WT background than in *cpk29-2*, whereas the *cpk29-2* mutant showed only a slight BFA-induced internalization of PINs (Figure 4, A and C). Similarly, the decrease in BFA compartments upon removal of BFA occurred more rapidly in WT than in *cpk29-2*, indicating that trafficking of PINs from endosomes to the PM was faster in WT than in the *cpk29-2* mutant background. This result suggests that CPK29 is required to promote the exocytic trafficking of PINs. Similar results were produced in BFA assays with WT and phospho-defective and -mimetic PIN1 and PIN2. Internal accumulation of phospho-defective PINs upon BFA treatment was slower than that of WT and phospho-mimetic forms, and BFA removal rapidly reduced the BFA compartments, with phospho-mimetic PINs experiencing the quickest decrease and phospho-defective PINs exhibiting the slowest (Figure 4, B and D). These results suggest that the conserved CPK29-target phosphorylation residues are involved in the exocytic trafficking of PIN1 and PIN2.

Next, fluorescence recovery after photobleaching (FRAP) analysis of PIN2 in root epidermal cells was used to further investigate the effects of CPK29 phosphorylation on PIN cycling. The FRAP rate of a PM protein can be affected by both lateral diffusion and exocytic delivery of the protein. However, polar proteins such as PINs have shown very limited lateral diffusion during FRAP compared to nonpolar proteins (Kleine-Vehn et al., 2011; Cho et al., 2012; Langowski et al., 2016; Ötvös et al., 2021). In particular, the lateral diffusion rate of PIN2 is negligibly low ($0.000138 \pm 0.0000285 \mu\text{m}^2 \text{s}^{-1}$ which is less than 1/1,000 of ATP-binding cassette G37 [ABCG37]; Langowski et al., 2016) so that FRAP analysis was adopted to show the exocytic delivery of PIN2 (Ötvös et al., 2021). In our FRAP analysis, the apical PIN2 signal recovery after photobleaching was significantly delayed in the *cpk29-2* mutant compared with the WT plant (Figure 4E). The phospho-defective PIN2 mutant also showed significant decreases in signal recovery at the apical PM of the root epidermal cell, whereas the recovery of phospho-mimetic PIN2 was significantly higher than those of WT and phospho-defective PIN2 (Figure 4F). Similar results were obtained with the FRAP analysis of PIN2 localized to the lateral PM (Supplemental Figure S10, A and B). On the other hand, the application of BFA together with

the peptide synthesis inhibitor cycloheximide (CHX) considerably inhibited the FRAP rate of PIN2 in the WT plant, indicating that a BFA-blockable exocytic recycling pathway indeed contributes to PIN2 recovery at the PM (Figure 4G). In contrast, BFA did not significantly further inhibit the PIN2 recovery in the *cpk29-2* mutant background, suggesting that BFA-sensitive exocytic trafficking of PIN2 is impaired in the mutant (Figure 4G). These data from PIN-trafficking analyses collectively suggest that CPK29-mediated phosphorylation of PIN2-HL facilitated PIN2 trafficking to the PM.

CPK29 was activated by Ca^{2+} and we, therefore, tested whether cellular Ca^{2+} depletion affected PIN trafficking. The apical polarity of PIN2 in the root epidermal cell was considerably hampered when seedlings were treated with Ca^{2+} antagonists such as LaCl_3 (Ca^{2+} -channel blocker) or EGTA (Ca^{2+} chelator) (Figure 4H), indicating that Ca^{2+} signaling was involved in proper PIN trafficking to the PM. CPK29 is likely to be one of the mediators in this signaling pathway. Collectively, these results support the idea that CPK29-mediated phosphorylation of PIN-HL promotes exocytic trafficking of PINs (Figure 4I).

CPK29 is required for PIN-mediated developmental processes

The CPK29-mediated modulation of PIN trafficking and polarity indicated that CPK29 could affect the dynamics of local auxin gradients and thus auxin-related development. Therefore, we next investigated auxin-related developmental processes, such as LR development, hypocotyl gravitropism, root twist, phyllotaxis, and floral organ formation and growth, in the *cpk29* mutant and in PIN mutants in which CPK29-target phosphorylation sites were mutated.

PAT plays multiple roles in LR development, from cell-fate determination to organogenesis and organ growth (Du and Scheres, 2018). Interestingly, *cpk29* mutants formed more LRs than WT, in which LR promotion was greater in a knockout *cpk29-2* mutant than in a knockdown *cpk29-1* mutant and was negated by the reintroduction of CPK29 into the mutant (Supplemental Figure S2, B and C; Figure 5A). The loss of CPK29 increased the number of LR primordia, particularly at Stages I and II (Figure 5B). Consistent with its LR promotion, loss of CPK29 enhanced the expression of several key LR-developmental genes such as GATA23, LBD16, and EXPA14 (Figure 5C). To determine how CPK29 affected early LR development, the dynamics of PIN polarity and auxin distribution during the early LR-developmental stages were examined. PIN1, which is anticlinally localized at stage I of the LR initial cells, begins to periclinally localize in the inner cell tier of the Stage II LR primordium (Benková et al., 2003; Figure 5D). This periclinal redistribution of PIN1 during Stage II was significantly impaired in the *cpk29-2* mutant (Figure 5, D and E). Accordingly, the ratio of auxin-sensitive DR5-directed signal between the outer and inner cells of Stage II LR primordia was significantly lower in the *cpk29-2* mutant than in WT (Figure 5, D and E), suggesting that PIN1-mediated lateral auxin transport from the inner

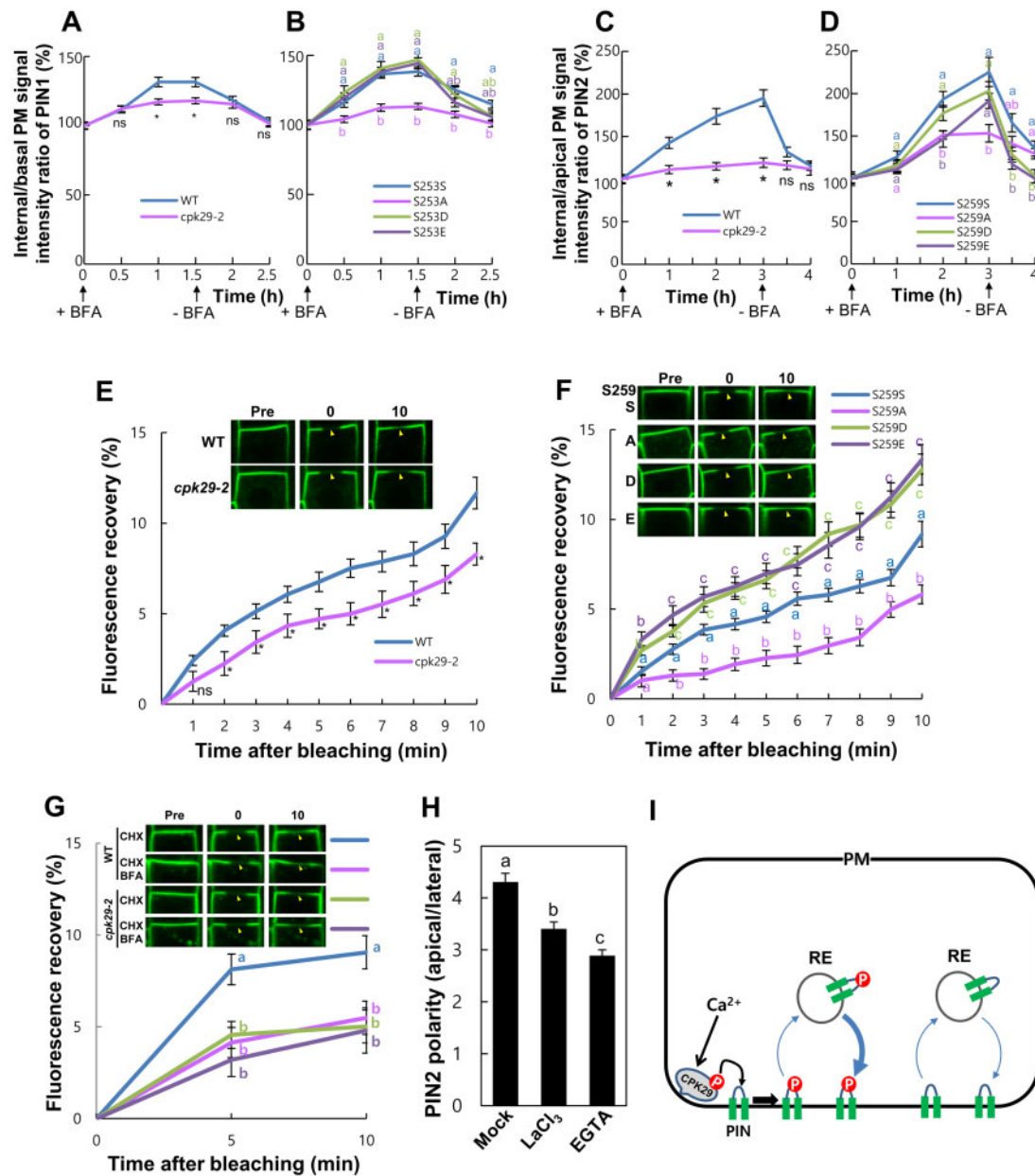


Figure 4 Phosphorylation of CPK29-target residues in PINs facilitates PIN recycling to the PM. A–D, Quantification of PIN trafficking behavior in response to the exocytic inhibitor BFA. WT PIN (*ProPIN::PIN::GFP*) was introduced into WT and *cpk29-2* mutant plants (A, C), and phospho-mutated versions of PIN were introduced into each *pin* mutant background (B, D). The relative PIN1 intensity ratio of internal vs. basal PM (A, B) and the relative PIN2 intensity ratio of internal versus apical PM (C, D) were estimated at the indicated time points. BFA (25 μ M) was applied (+ BFA) or washed out (–BFA) at the time points indicated by arrows. Seedlings were pretreated for 30 min and co-treated with CHX (50 μ M). Data represent means \pm SE ($n = 61$ –76 cells in A, 50–65 cells in B, 46–85 cells in C, and 47–74 cells in [D]) from at least two independent transgenic lines for each construct). E–G, Kinetics of FRAP of WT PIN2 in WT and *cpk29-2* backgrounds (E) and phospho-mutated versions of PIN2 (F) and the BFA effects on PIN2 FRAP (G) in root epidermal cells. Treatments of BFA and CHX (G) were done as in A–D. Data represent means \pm SE ($n = 66$ –75 cells in E, 46–77 cells in F) from at least two independent transgenic lines for each construct, and 19–39 cells in G). Insets show representative confocal images before (Pre) and after (0 and 10 min) photobleaching (4- μ m wide). Arrowheads indicate photobleached regions. (H) Effect of Ca²⁺ antagonists on PIN2 polarity in root epidermal cells (apical versus lateral PM). Data represent means \pm SE ($n = 157$ –230 cells from 9–15 roots). I, Model illustrating that CPK29-mediated PIN phosphorylation facilitates PIN-recycling pathway. P, phosphate; RE, recycling endosome. Different letters denote significant differences (B, D, and F–H; ANOVA test, $P < 0.05$), and the asterisk indicates significant difference from the WT value ($P < 0.001$ [A, C] and $P < 0.05$ [E], Student's *t* test; ns, not significant).

to the outer cell decreased in the mutant. In contrast, PIN1 polarity and auxin distribution did not show significant differences between WT and the *cpk29-2* mutant in Stages I

and III (Figure 5, D and E), implying that the CPK29 function specifically affected Stage II. This was consistent with CPK29 expression, which was confined to a narrow spatiotemporal

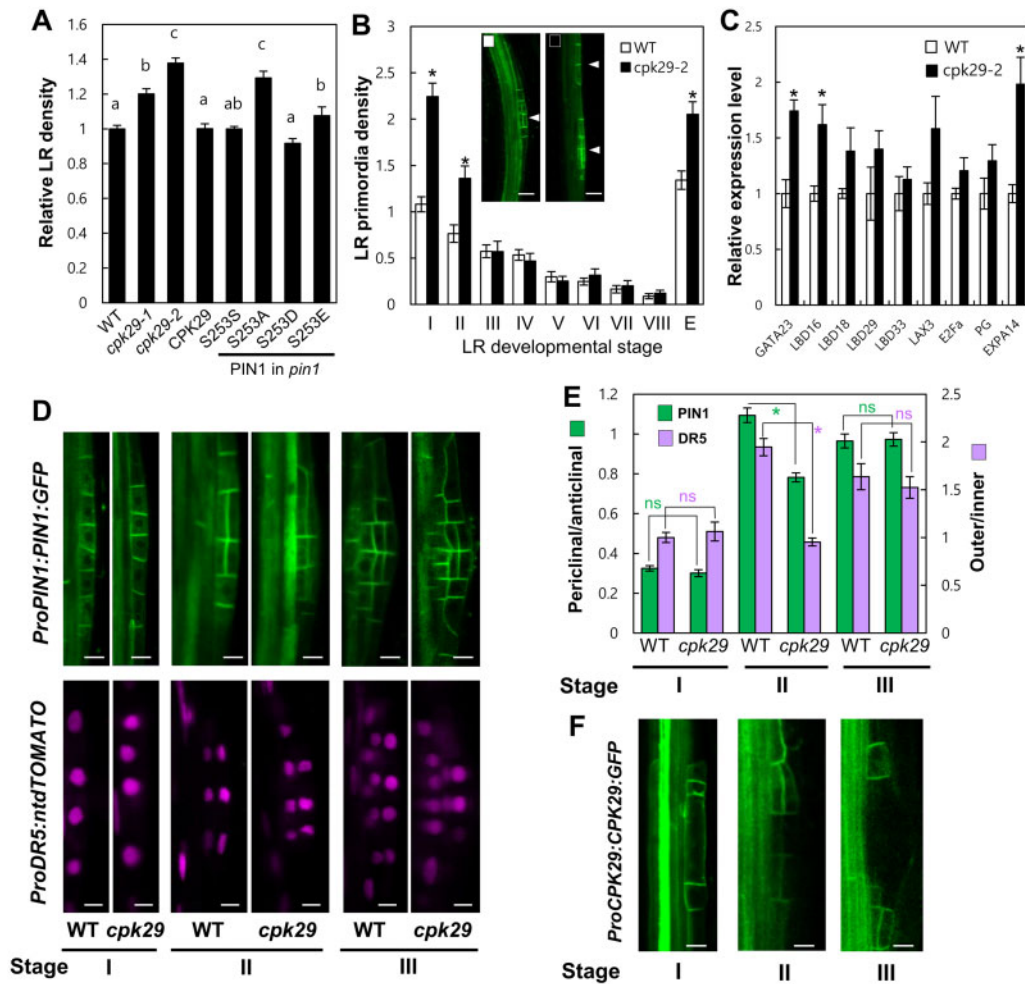


Figure 5 CPK29 is involved in LR development. A, Relative LR densities (numbers of emerged LR per cm of root) of WT, *cpk29* mutants, *ProCPK29:CPK29:GFP* in *cpk29-2* (CPK29), and *ProPIN1:PIN1:GFP* transgenic lines expressing phospho-mutated versions of PIN1 in the *pin1* background. Data represent means \pm SE ($n = 46$ –261 seedlings from 3–4 independent transgenic lines). Different letters denote significant differences (ANOVA test, $P < 0.05$). B, Distribution of LR primordia density at different developmental stages in WT and *cpk29-2* ($n = 18$ –24 seedlings; *, significantly different from the WT value, $P < 0.001$, Student's *t* test). 'E' indicates emerged LR primordia. Arrowheads in the inset indicate LR primordia revealed by *ProPIN1:PIN1:GFP* expression. Bar = 20 μ m. C, Relative transcript levels of LR-related genes in the WT and *cpk29-2* mutant. Data represent means \pm SE of at least three independent biological replications. (*, significantly different from the WT value, $P < 0.05$, Student's *t* test). D, Confocal images of *ProPIN1:PIN1:GFP* and *ProDR5:ntdTOMATO* in Stages I and III LR primordia of WT and *cpk29-2* (*cpk29*). Bar = 10 μ m. E, Ratios of periclinal/anticlinal PIN1 intensity (green bar) and outer/inner cell tier *ntdTOMATO* (DR5) intensity (red bar) in LR primordia of WT and *cpk29-2* as described in (D). Data represent means \pm SE ($n = 33$ –72 cells from 6 to 14 seedlings, * $P < 10^{-10}$, Student's *t* test for PIN1; $n = 15$ –33 cells from 8 to 11 seedlings from at least three independent transgenic lines for each construct, * $P < 10^{-14}$, Student's *t* test for DR5; ns, not significant). F, Localization of CPK29 (*ProCPK29:CPK29:GFP*) in stage I–III LR primordia. Bar = 10 μ m.

window during LR primordial development, namely, to the Stages I and II LR primordial initials (Figure 5F). During Stage I, CPK29 localized to both the apical/basal and periclinal sides, but this localization pattern began to disperse at the central LR primordium area from Stage II and was almost completely dissipated from Stage III onward, leaving only some residual expression at the basal periphery of the primordium (Figure 5F). This observation led us to hypothesize that periclinally localized CPK29 in Stages I and II primordial cells may be involved in the establishment of the first periclinal PIN1 polarization. Defects in initial periclinal PIN1 localization from the loss of CPK29 could lead to more auxin accumulation in the inner cell tier (or less in the outer cell

tier) of the Stage II LR primordium (Figure 5, D and E), which could, in turn, result in a transient arrest of Stages I and II or an increase in primordium number at these stages.

The *cpk29-2* mutant root showed a more twisted growth pattern than WT, as represented by the rotation of the root epidermal cell file along the longitudinal root axis, and this was rescued by reintroduction of the CPK29 gene into the mutant (Figure 6, A and B). The *pin2* mutant showed a similar phenotype, and the introduction of phospho-defective or -mimetic PIN2 forms could not rescue the *pin2* mutant phenotype (Figure 6, A and B). The root-twist degree of *pin2 cpk29-2* double mutant was not significantly different from that of each single mutant, indicating that PIN2 and

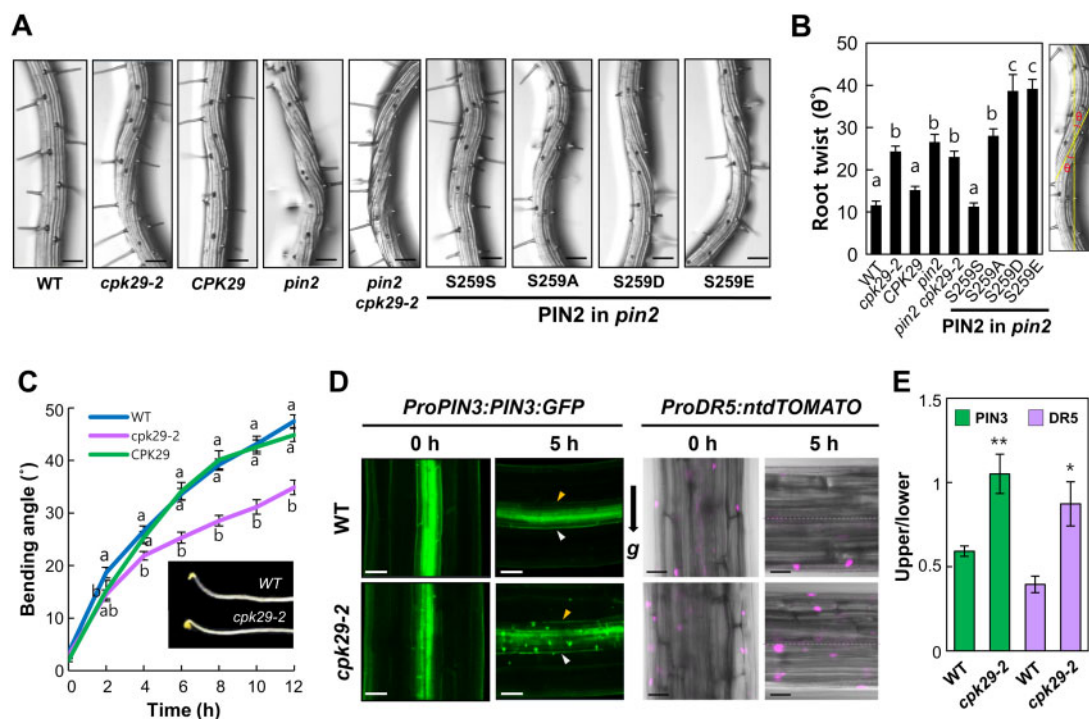


Figure 6 CPK29 is implicated in PIN2-mediated modulation of root twist and PIN3-mediated hypocotyl gravitropism. **A**, Representative root images of WT, *cpk29-2* mutant, *ProCPK29:CPK29:GFP* in *cpk29-2* (CPK29), *pin2* mutant, *pin2 cpk29-2* double mutant and *ProPIN2:PIN2:GFP* lines expressing phospho-mutated versions of PIN2 in *pin2*. Bar = 100 μ m. **B**, Root twist degrees of the plants shown in **A**. Root twist is represented by the angle θ formed by the root longitudinal axis and the epidermal cell file axis. Data represent means \pm SE ($n = 9$ –36 roots from 2 to 6 independent lines for each construct; different letters denote significant differences [ANOVA test, $P < 0.05$]). **C**, Hypocotyl gravitropic kinetics of WT, *cpk29-2*, and a complementation line expressing *ProCPK29:CPK29:GFP* in *cpk29-2* (CPK29) after gravistimulation. Data represent means \pm SE ($n = 21$ –96 seedlings). The inset shows representative hypocotyl images of WT and *cpk29-2* 12 h after gravistimulation. **D**, Confocal images of WT and *cpk29-2* hypocotyls showing the subcellular localization and expression of *ProPIN3:PIN3:GFP* and *ProDR5:ntdTOMATO* at 0 and 5 h after gravistimulation. The arrow indicates the direction of gravity (g). Arrowheads indicate the PIN3:GFP signal at the upper (orange) and lower (white) outer PM of the starch sheath cell. The central dashed lines divide upper and lower parts of the hypocotyl region. Bar = 50 μ m. **E**, Ratios of upper/lower signals of PIN3:GFP at the outer PM of the starch sheath cell and ntdTOMATO (DR5) in the hypocotyl 5 h after gravistimulation as shown in **D**. Data represent means \pm SE ($n = 39$ –42 cells from 25 to 34 roots for PIN3, and 34 cells from 23 to 26 roots for DR5 from 3 to 5 independent transgenic lines for each construct; asterisks significantly different from the WT value, * $P < 0.005$ and ** $P < 0.001$, Student's *t* test).

CPK29 would take a linear genetic pathway to affect root twist/untwist (Figure 6, A and B). The decrease in PIN2 protein level and subsequent defects in shootward auxin transport in the root are likely implicated in root skewing (Qi and Zheng 2013). The apical PIN2 polarity in the root epidermal cell was partially compromised by the loss of CPK29 and by the mutations in CPK29-target residues of PIN2 (Figure 3, C and D). The polarity defect of phospho-mutated PIN2 could affect shootward auxin transport from the root tip and cause twisting of the root. The *cpk29-2* mutant, however, did not exhibit significant defects in root gravitropism which was also known to be affected by PIN2 activity. The loss of CPK29 did not completely disrupt the apical PIN2 polarity in the mutant root epidermal cell where the apical PIN2 level still doubled the lateral PIN2 level (Figure 3, C and D). This level of PIN2 polarity could be enough to operate normal root gravitropism but insufficient to keep the root untwisted. On the other hand, PIN2-involving root twist/untwist and root gravitropism may take different mechanistic pathways downstream of

auxin (or of PAT). The spatial separation of two developmental phenomena might reflect this notion; root twist occurs from the late elongation zone throughout the differentiation zone, but gravitropic root bending occurs at the early elongation zone of the root.

Hypocotyl gravitropism was partially impaired in the *cpk29-2* mutant, and this was rescued by the reintroduction of CPK29 into the mutant (Figure 6C). Upon gravi-stimulus, PIN3 re-localized downward in the gravitational direction in the hypocotyl starch sheath cell (Figure 6, D and E), as reported previously (Rakusová et al., 2011). However, PIN3 re-localization was significantly hampered in the *cpk29-2* mutant (Figure 6, D and E). Accordingly, auxin redistribution in the gravitational direction, as shown by DR5-promoted signal activity, was considerably reduced in the mutant background (Figure 6, D and E), suggesting that CPK29-mediated modulation of PIN3 polarity was involved in hypocotyl gravitropism.

PIN1-mediated phyllotaxis and reproductive organ development also showed defects in the *cpk29-2* mutant and

with phospho-mutations of the CPK29-target sites in PIN1-HL. The phyllotaxis of vegetative leaves was considerably disrupted by the loss of *CPK29*, and this mutant phenotype was rescued by the reintroduction of *CPK29* under its own promoter (Figure 7). However, the transformant in which *CPK29* was introduced under the control of the 35S promoter retained the disrupted phyllotactic phenotype, indicating that the *CPK29*-expressing domain was critical to modulation of PIN1-mediated phyllotaxis. Normal phyllotaxis was restored by the reintroduction of WT PIN1 but not by the introduction of phospho-defective or -mimetic versions of PIN1 into the *pin1* mutant (Figure 7). The failure of phyllotactic restoration by the phospho-mimetic PIN1 was likely due to the impaired subcellular polarity of this version of PIN1 (Figure 3, A and B). Similarly, the introduction of phospho-defective and -mimetic PIN1 forms into the *pin1* mutant did not restore normal reproductive organ development such as floral patterning and fruit setting (Figure 8).

While phospho-defective and -mimetic PINs generated opposite phenotypes in PIN trafficking (namely, slow and fast PIN recycling by phospho-defective and mimetic mutation, respectively; Figure 4), both phospho-mutant forms resulted in similar developmental phenotypes such as root twist, phyllotaxis, and reproductive development (Figures 6–8). The latter likely resulted from the similar disruption of PIN polarity by both phospho-mutations, though it was observed in root tissues (Figure 3, A–D). Compared to the WT PINs, the active exocytic behavior of phospho-mimetic PINs (Figure 4F) could cause more lateral exocytosis of PINs, which would lower the relative apical or basal PIN polarity.

Discussion

The HL region between residues 200–300 of long PINs carries phosphorylation hot spots that are targeted by the aforementioned protein kinases and that are fundamental for PIN trafficking (Barbosa et al., 2018; Supplemental Figure S11). Our results showed that Ca^{2+} signaling-mediated modulation of PIN trafficking involved a specific phosphorylation code on the PIN-HL. Among the known PIN-phosphorylating protein kinases, AGC-type protein kinases (PID/WAGs, D6PK, and AGC1–12) mostly share common phosphorylation sites, termed S1–S5 (Dhonukshe et al., 2010; Huang et al., 2010; Ganguly, Lee, et al., 2012; Weller et al., 2017; Supplemental Figure S11). However, the ‘Sc’ site (Ser targeted by CPK29, i.e. S253 in PIN1 and S259 in PIN2) was not phosphorylated by AGC-type or any other type of kinases other than CPK29 (as summarized in Supplemental Figure S10). This suggests that the Sc phospho-site is specific to CPK29 and thus the site is likely to mediate Ca^{2+} -signaling for the modulation of PIN trafficking. In addition, the 3 mL and M3 sites (Ganguly, Lee, et al., 2012; Sasayama et al., 2013; Ki et al., 2016; Supplemental Figure S11) and two TPRXS motifs (Dhonukshe et al., 2010; Huang et al., 2010; Zourelidou et al., 2014; Haga et al., 2018) were targeted by

an AGC kinase but not by CPK29 (Figure 1, D and G). These data further indicated that the target phosphorylation sites in the PIN-HL have been specified between AGC kinases and CPK29.

Although CRKs are not directly activated by Ca^{2+} , they may also mediate Ca^{2+} signaling for PIN modulation. However, CRK5—the only CRK known to modulate PIN trafficking—exhibited quite distinctive characteristics to those shown by CPK29. CRK5 actively recycles between endosomes and PM, as it easily forms internal compartments after BFA treatment (Rigó et al., 2013). In contrast, BFA treatment did not cause the formation of compartments containing CPK29, indicating that CPK29 scarcely underwent BFA-sensitive recycling (Figure 2D; Supplemental Figure S7B). Moreover, while CPK29 generally modulated the trafficking of all major long PINs, CRK5 affected the trafficking of PIN2 only, and not the trafficking of other auxin transporters such as AUX1, PIN1, PIN3, PIN4, and PIN7 (Rigó et al., 2013). Considering that PINs and PIN-phosphorylating AGC kinases and CRK5 take the recycling pathway (Geldner et al., 2001; Lee and Cho, 2006; Rigó et al., 2013; Barbosa et al., 2014) but CPK29 does not, those AGC kinases and CRK5 may also target their substrates during the recycling process whereas CPK29 is likely to act on them mostly at the PM.

CPKs are involved in various biological processes, and among their substrates included are membrane transporter proteins such as channels for ions and water and Ca^{2+} pump. *In vitro* and *in vivo* phosphorylation investigations have revealed many kinase/substrate relationships between CPKs and membrane transporters; CPK6 and CPK23/SLOW ANION CHANNEL-ASSOCIATED 1 (Geiger et al., 2010; Brandt et al., 2012; Maierhofer et al., 2014), CPK3, CPK4, CPK5, and CPK11/vacuolar TWO-PORE K^{+} -CHANNEL 1 (TPK1; Latz et al., 2013), CPK13/ K^{+} -channels KAT1/2 (Ronzier et al., 2014), CPK34/ Ca^{2+} -channel CNGC18 (Curran et al., 2011), CPK34/aquaporins NIP4;1 and NIP4;2 (Di Giorgio et al., 2016), and CPK16/ Ca^{2+} -ATPase ACA8 (Giacometti et al., 2012). These CPKs are from all over the major CPK subgroups but not from a specific subgroup, implying that different lineages of CPKs have been functionally converged to have membrane transporters as substrates.

The biological function of CPK29 has been little characterized. *CPK29* expression is induced by salt stress, and CPK29 was shown to phosphorylate the N-terminus of TPK1 *in vitro* (Latz et al., 2013), which, however, requires *in vivo* confirmation due to different subcellular localizations between CPK29 (PM) and TPK1 (vacuolar tonoplast). When co-expressed with *CPK28* under a constitutive promoter, *CPK29* and *CPK28* enhanced drought tolerance of Arabidopsis plants, though the expression of every single gene showed no prominent effect (Schulz et al., 2021).

Our study reveals auxin-transporting PINs as targets of CPK29. With regard to the formation of auxin gradients, CPK29 may act as a general modulator for exocytic PIN

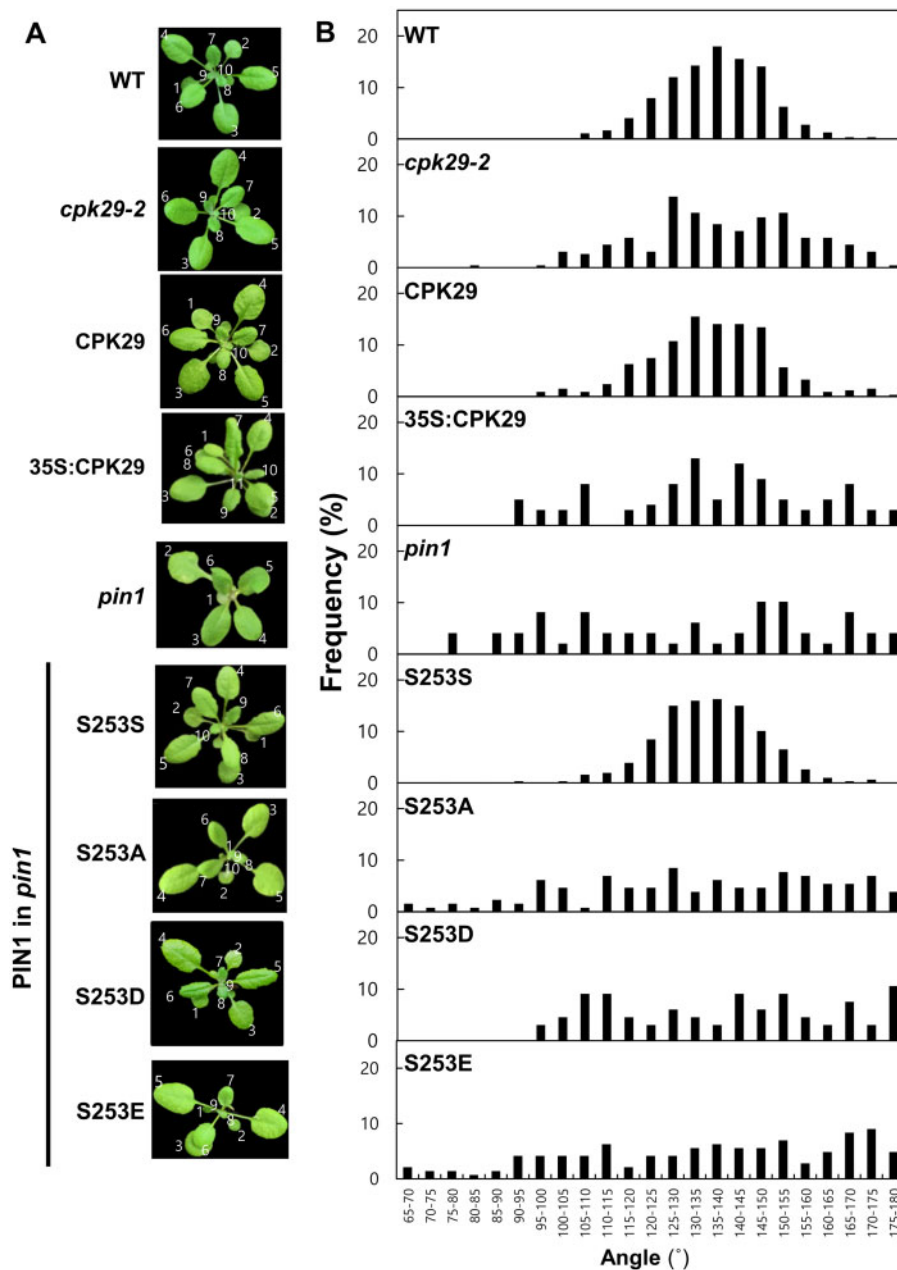


Figure 7 CPK29 is involved in PIN1-mediated phyllotaxis. A, B, Images of rosette leaves (A) and the frequency of phyllotatic angles (B) of WT, *cpk29-2* mutant, *ProCPK29:CPK29:GFP* in *cpk29-2* (CPK29), *Pro35S:CPK29:RFP* in WT (35S:CPK29), *pin1* mutant, and *ProPIN1:PIN1:GFP* transgenic lines expressing phospho-mutated versions of PIN1 in the *pin1* background. $n = 12\text{--}25$ plants from 4 to 6 independent lines for each construct in case of transformants.

trafficking in response to Ca^{2+} signals, as it is expressed ubiquitously in diverse organs, targets multiple major long PINs, and affects various auxin-related developmental processes such as LR development, root twist, hypocotyl gravitropism, phyllotaxis, and floral organ development. Although some of these developmental processes are physiologically linked to Ca^{2+} signaling (Toyota et al., 2008; Chen and Kao, 2012), our study suggests CPK29 as the molecular linker between Ca^{2+} and PAT and opens a possibility that more diverse PAT-involved biological processes could be modulated by Ca^{2+} signaling.

Materials and methods

Plant materials and growth conditions

Arabidopsis thaliana Columbia ecotype (Col-0) plants were used as WT and for transformation with transgene constructs unless otherwise stated. Two loss-of-function mutants, *cpk29-1* and *cpk29-2*, were obtained from the Arabidopsis Stock Center (<http://www.Arabidopsis.org/>). Seeds were cold-treated at 4°C for 4 days before germination and cultivation at 22°C under a 16-h light/8-h dark photoperiod with fluorescent illumination (FHF 325S-EXD; Kumho Electric, Korea), with a light

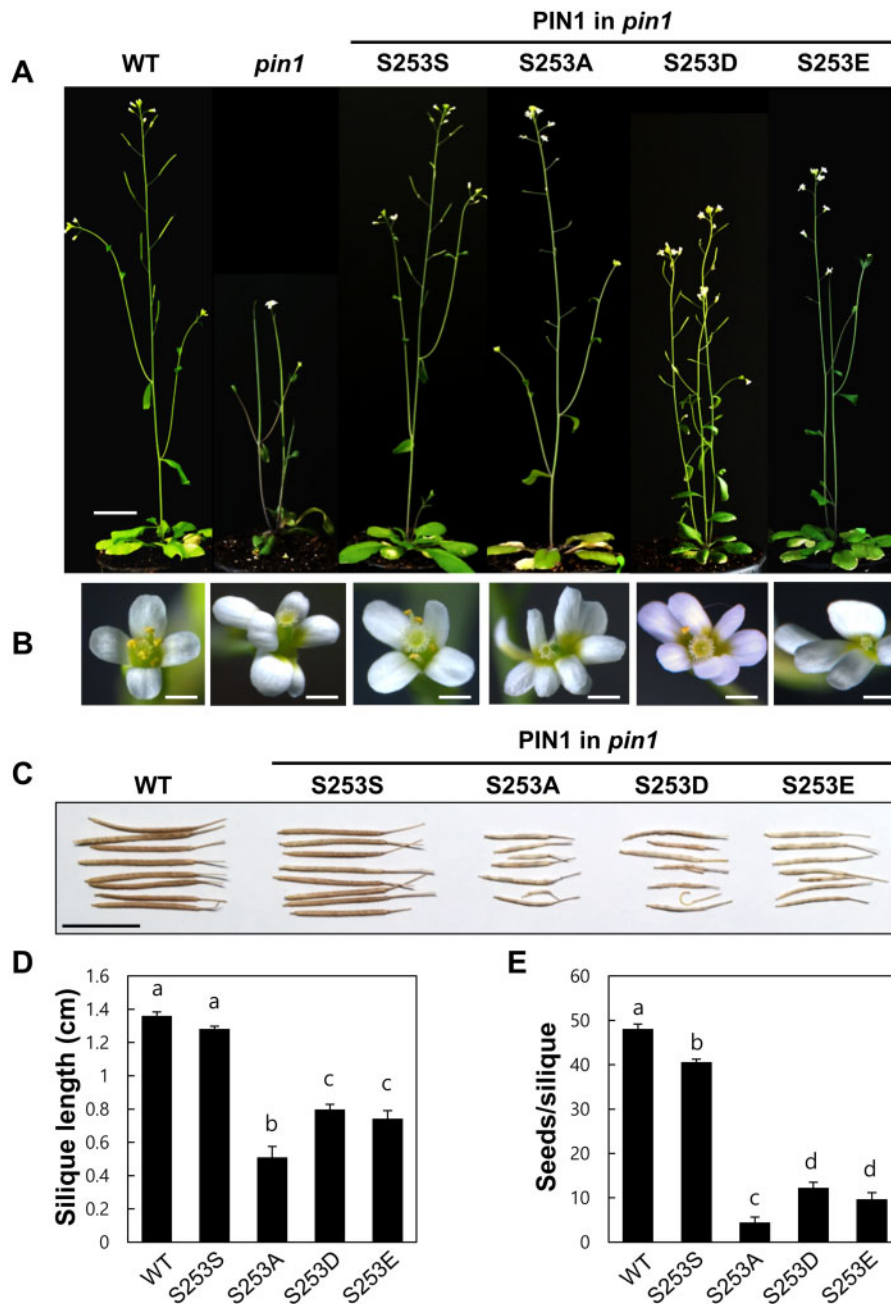


Figure 8 The CPK29-target residue in PIN1 is necessary for PIN1-mediated reproductive development. A, B, Inflorescence stem (A) and floral organ (B) phenotypes of WT, *pin1*, and *ProPIN1:PIN1:GFP* transgenic lines expressing phospho-mutated versions of PIN1 in the *pin1* background. Bar = 2 cm (A) and 1 mm (B). C, Silique phenotypes of WT and *ProPIN1:PIN1:GFP* transgenic lines expressing phospho-mutated versions of PIN1 in the *pin1* background. Bar = 1 cm. D, E, Silique length and seed number per silique of WT and *ProPIN1:PIN1:GFP* transgenic lines expressing phospho-mutated versions of PIN1 in the *pin1* background. Data represent means \pm SE ($n = 8\text{--}38$ siliques [D] and 22–54 siliques [E] of 3–8 plants from 3 to 6 independent transgenic lines for each construct; different letters denote significant differences [ANOVA test, $P < 0.05$]).

intensity of $130 \mu\text{mol m}^{-2} \text{s}^{-1}$. Seedlings were grown on agar plates containing 4.3 g L^{-1} Murashige and Skoog (MS) nutrient mix (Duchefa, the Netherlands), 1% sucrose, 0.5 g L^{-1} MES (pH 5.7 with KOH), 0.8% agarose (SeaKem, Cambrex BioScience Rockland). Arabidopsis plants were transformed by the floral dip method using *Agrobacterium tumefaciens* strain C58C1, and transformants were selected on agar plates containing hygromycin ($30 \mu\text{g mL}^{-1}$) or

phosphinothricin ($30 \mu\text{g mL}^{-1}$) and cefotaxime ($10 \mu\text{g mL}^{-1}$). Four-day-old seedlings were analyzed unless stated otherwise.

For the genetic analysis between *pin2* and *cpk29-2* for the root twist phenotype, *pin2* (*eir1-1*) and *cpk29-2* were crossed, and the homozygous double mutant was used for the genetic analysis. The genotype of the homozygous double mutant was confirmed by observation of root

agravitropism and genomic DNA sequencing after PCR of the mutated region (for *pin2*) and by identifying the T-DNA insertion (for *cpk29-2*).

Transgene constructs

For bacterial protein expression, which was used for *in vitro* protein pulldown and phosphorylation assays, *PIN*-HLs (*PIN1*, 167–460 amino acids; *PIN2*, 167–485; *PIN3*, 167–478) and *CPK29* cDNAs were obtained and amplified from Arabidopsis seedling mRNA using the primer sets listed in Supplemental Table S4 (hereafter all PCR primers are listed in this Table) and cloned into the *Bam*HI/*Sal*I sites of the *pGEX-4T-1* vector (GE Healthcare, Incheon, Korea) for generation of fusion proteins with glutathione *S*-transferase (GST) at their N-termini. Phospho-mutated *PIN*-HLs and *CPK29* were generated by mutagenesis using the mega-primer PCR method. For single-mutated constructs, a mutated primer was used for the first PCR, and this mutated PCR product was used as a (mega) primer in the second PCR to obtain the final mutated construct, which was cloned into the *Bam*HI/*Sal*I sites of *pGEX-4T-1*. For double site-mutated *PIN*-HLs constructs, a second mutated primer was used in the mega-primer PCR with the first mutated construct as a template. The constructs for the 3m1 and M3 phospho-mutants of *PIN1* and GST:*PID* were as previously described (Ganguly, Lee, et al., 2012; Ki et al., 2016). For the construct used in *in vitro* pulldown assay, cDNA of *CPK29* was cloned into the *Eco*RI/*Sal*I sites of *pET-30a-c(+)* (Novagen).

Binary vectors *pCAMBIA1300-NOS* and *pCAMBIA3300-NOS*, with modified cloning sites (Lee et al., 2010), were used to assemble transgenes for Arabidopsis transformation. The *ProPIN1:PIN1:GFP* (Ki et al., 2016), *ProPIN2:PIN2:GFP* (Xu and Scheres, 2006), and *ProPIN3:PIN3:GFP* (Ganguly, Lee, et al., 2012) constructs were as previously described. Site-directed mutagenesis of the phosphorylation sites of *PIN1* (S253) and *PIN2* (S259) was performed using the mega-primer PCR method described above, using the *ProPINs:PINs:GFP* constructs, including WT genomic *PIN* sequences, as templates. Mutagenized *PINs* were cloned into the *Sal*I/*Nco*I and *Sal*I/*Avr*II sites, respectively, for *PIN1* and *PIN2*, to generate *ProPINs:mPINs:GFP* constructs. To construct *ProCPK29:CPK29:GFP*, the 716 bp *CPK29* promoter, and 2703 bp *CPK29* coding region (with stop codon removed) were amplified from Arabidopsis genomic DNA and sequentially inserted into the *Hind*III/*Sal*I and *Kpn*I/*Apal* sites of the binary vector, respectively. The *GFP* region was amplified from *ProE7:GFP* (Kim et al., 2006) and cloned into the *Asc*I site, downstream of *ProCPK29:CPK29*. For the *ProCPK29:GUS:GFP* construct, the *GUS* fragment (with stop codon removed) was amplified from the *pBI101* vector (Clontech) and cloned into the *Pac*I/*Avr*II sites downstream of the *ProCPK29*—including vector described above. The *GFP* region from *ProCPK29:CPK29:GFP* was amplified and inserted into the *Avr*II/*Asc*I sites downstream of *ProCPK29:GUS*. For *Pro35S:CPK29:RFP*, *Pro35S* was obtained by enzyme digestion (*Hind*III/*Sal*I) from *Pro35S:PGP4:YFP* (Cho et al., 2007) and inserted into the same digestion sites of *pCAMBIA1300-NOS*.

Next, the genomic *CPK29* coding region from *ProCPK29:CPK29:GFP* was cloned into the *Kpn*I/*Apal* sites. The red fluorescence protein (*RFP*) coding region was obtained from *ProE7:PGP4:RFP* (Cho et al., 2007) and inserted into the *Asc*I/*Spe*I sites of the binary vector. For the *ProDR5:ntdTOMATO* constructs, the *ProDR5v2* and *ntdTOMATO* coding regions were PCR-amplified using the *pGreenIIIM DR5v2:ntdTomato/DR5:n3GFP* vector (a gift from Dolf Weijers; Liao et al., 2015) as a template, and inserted into the *Asc*I and *Xba*I sites, respectively.

Bacterial protein expression and *in vitro* protein pulldown

Plasmids were transformed into *Escherichia coli* BL21-DE3 Rosetta competent cells (Novagen), and protein expression was induced with 1 mM isopropyl β -D-1-thiogalactopyranoside (IPTG) for 4 h. Cells were lysed with Thermo Scientific Pierce B-PER Bacterial Protein Extraction Reagents, comprising 1 mL B-Per, 2 μ L DNase1 (5 unit μ L⁻¹), 20 μ L lysozyme (10 mg mL⁻¹), and 1 \times protease inhibitor cocktail (Roche). For the pulldown experiment to obtain *PIN2*-HL-interacting proteins (PIPs), 40 μ L glutathione sepharose beads 4B (GE Lifesciences) were incubated first with \sim 10 μ g GST or GST:*PIN2*-HL fusion protein at 4°C on a shaker (10 rpm) for 4–6 h to allow binding. For whole-cell plant extracts, 7-day-old Col-0 seedlings were homogenized in a mortar using lysis buffer (50 mM Tris-HCl pH 7.5, 100 mM NaCl, 0.1% Triton-X 100, 0.5% NP-40, 1 \times protease inhibitor cocktail [Roche], 1 mM phenylmethylsulfonyl fluoride [PMSF], and 10% glycerol). The homogenate was then centrifuged twice at 10,000 \times g for 10 min, and the supernatant was collected. For pulldown of PIPs, plant protein extracts (100 μ g total) were added to the GST- or GST:*PIN2*-HL-bound sepharose beads and the mixtures were incubated at 4°C for 3 h. The beads were then washed with phosphate-buffered saline (PBS with 0.1% Tween-20) six times, after which proteins were eluted with 100 μ L glutathione elution buffer (50 mM Tris-HCl, 30 mM reduced glutathione pH 8.0). Elution fractions were then separated using 10% SDS-PAGE gel electrophoresis, and distinct bands were excised from the gel and used for trypsin digestion and mass spectrometry analysis.

For *in vitro* pull-down experiments between *CPK29* and *PIN1*-, *PIN2*-, and *PIN3*-HL, His-tagged *CPK29* (His:*CPK29*) and GST:*PIN*-HLs were expressed in the *E. coli* cells as described above. Fifty microliter glutathione sepharose beads 4B (GE Lifesciences) were incubated first with \sim 10 μ g GST or GST:*PINs*-HL for 3 h at 4°C on a rotator (15 rpm) to allow binding. After removing the supernatants, the beads were incubated with \sim 10 μ g His:*CPK29* protein for 2 h at 4°C on a rotator (15 rpm) for interaction. The beads were then washed 5 times with 1 \times Tris-buffered saline (TBS, including 0.1% [v/v] Tween-20) to remove nonspecifically bound proteins. Bound proteins were isolated from the beads by adding 1 \times SDS loading dye, separated by SDS-PAGE, transferred to 0.45 μ m nitro-cellulose membranes

(GE Lifesciences), and probed with 1:3000 diluted anti-His (MBL, cat. # D291-3) and anti-GST antibodies (Abcam, cat. # AB3416). Chemiluminescence detection was performed with ECL (LPS solution) protein gel blotting substrate in a chemiluminescence imaging system (Davinch-chem).

Liquid chromatography-tandem mass spectrometry analysis

Liquid chromatography-tandem mass spectrometry (LC–MS/MS) analysis was used to identify CPK29 and PIN-HL phosphorylation sites. Protein samples were prepared as follows: ~1 µg GST:CPK29 or GST:mCPK29 and GST:PIN-HLs were incubated in kinase buffer (20 mM Tris–HCl pH 7.5, 10 mM MgCl₂, 10 mM EGTA, and 10 mM CaCl₂) with 200 µM ATP in a total volume of 20 µL for 1 h at 22°C. Samples were stored at 4°C to prevent additional protein phosphorylation. The soluble mixtures were denatured with 8 M urea in 50 mM ammonium bicarbonate (ABC), followed by reduction and alkylation of cysteine thiols. After dilution to a urea concentration of 1 M with 50 mM ABC buffer, proteins were digested with trypsin overnight at 37°C. LC–MS/MS using high-energy collision dissociation fragmentation was performed on Orbitrap Q-Exactive or Orbitrap Fusion Lumos mass spectrometers (Thermo Fisher Scientific) coupled to a nanoACQUITY UPLC (Waters) instrument equipped with an in-house packed capillary trap column (150 µm internal diameter, 3 cm) and an analytical column (75-µm internal diameter, 100 cm) with 3 µm Jupiter C18 particles (Phenomenex) at a flow rate of 300 nL min⁻¹. The acquired dataset was searched using the MS-GF+ (version 2017 January) algorithm at 10 ppm of precursor ion mass tolerance with variable phosphorylation modification parameter (+ 79.966 Da) on Ser/Thr/Tyr residues against the *A. thaliana* UniProt proteome database with 1% protein false discovery rate.

The *in vivo* identification of the phosphorylation sites in CPK29 and PINs by LC–MS/MS analysis was performed as previously described (Yang et al., 2013). Four-day-old WT Arabidopsis seedlings were homogenized using mortar and pestle with urea extraction buffer (150 mM Tris–HCl [pH 7.6], 8 M urea, 0.5% SDS, 1.2% Triton X-100, 20 mM EDTA, 20 mM EGTA, 50 mM NaF, 1% glycerol 2-phosphate, 1 mM PMSF, 5 mM DTT, 0.5% phosphatase inhibitor mixture 2 [Sigma], an EDTA-free protease-inhibitor mixture [Complete], 5 mM ascorbic acid, and 2% polyvinylpyrrolidone). The homogenates were then centrifuged at 10,000g for 1 h to obtain the supernatant which was then subjected to ultracentrifugation at 110,000g for 2 h. The supernatant was mixed with acetone/methanol (12:1 v/v), and the protein pellet was rinsed with acetone:methanol:H₂O (12:1:1.4 v/v/v) twice. The protein pellet was resolved with resuspension buffer (50 mM Tris–HCl [pH 6.8], 8 M urea, 1% SDS, 10 mM EDTA, and 5 mM DTT), and C18 cleanup and lyophilization were conducted. The phosphopeptides were enriched with

High-select Fe-NTA & TiO₂ Phosphopeptide Enrichment Kit (Thermo Scientific) before the LC–MS/MS analysis.

In vitro phosphorylation assay

GST-fused kinases and protein substrates were acquired as described above. For *in vitro* phosphorylation assays, ~1 µg GST:CPK29 (or GST:PID) and substrate proteins were added to 20 µL kinase buffer (10 mM Tris–HCl pH 7.5, 10 mM MgCl₂, 1 mM EGTA, and a range of CaCl₂ concentrations). [Ca²⁺]_{free} values were calculated using <https://web.stanford.edu/~cpatton/webmaxc/webmaxcE.htm>. The kinase buffer also included 1 µCi [γ-³²P] ATP. The reaction was incubated for 1 h at 22°C and then halted by adding 5 µL SDS–PAGE loading buffer and boiling for 5 min. The reaction samples were then separated using 10% SDS–PAGE gel electrophoresis and stained with Coomassie Brilliant Blue (CBB). Phosphorylation analysis with PID and PIN1-HL was performed as described previously (Huang et al., 2010). Autoradiography was performed using BAS imaging plates (BAS 2040, Fujifilm) and a Bio-imaging Analyzer (BAS-2500, Fujifilm). Phosphorylation intensity was estimated using ImageJ 1.50b software (National Institutes of Health). Phosphorylation intensity of separated protein bands was estimated by subtracting the intensity of the region immediately surrounding the band and normalizing it to the CBB staining intensity.

Sequence alignment and phylogenetic analysis

Amino acid sequences were aligned using CLUSTAL W with the default parameters (gap penalty, 10.0; gap length penalty, 0.2; delay divergent seqs, 30%). Phylogenetic trees were generated by the Neighbor-Joining method with Poisson model using the MEGA version 7 software package after CLUSTAL W alignment of the whole amino acid sequences. The number of bootstrap replicates was 1,000. Tree branches indicate the number of amino acid substitutions per site as shown by the scale bar.

Histological observation of β-glucuronidase activity

Glucuronidase (GUS) analysis was performed as described previously (Cho and Cosgrove, 2002). Seedlings and plant parts were incubated in GUS reaction buffer (1 mM 5-bromo-4-chloro-3-indoyl-β-D-glucuronide cyclohexylammonium salt, 0.1 M NaH₂PO₄, 0.01 M EDTA, 0.1% Triton X-100, and 0.5 mM potassium ferricyanide pH 7) for 3 h at 37°C and then destained in 70% ethanol. Images were obtained using an M205 FA stereomicroscope (Leica).

Membrane protein isolation

Membrane protein isolation was performed as previously described (Ganguly, Lee, et al., 2012) with modifications. Seven-day-old Arabidopsis seedlings were homogenized using mortar and pestle with isolation buffer (0.25 M sorbitol, 50 mM HEPEPS-KOH pH 7.5, 1 mM EGTA, 1 mM EDTA, 1 mM MgCl₂, 5% [v/v] glycerol, 1% [w/v] polyvinylpyrrolidone, 2 mM DTT, 1 mM PMSF, and protease inhibitor cocktail [Sigma]). The homogenates were then centrifuged at 8,000g

for 10 min to obtain the supernatant (cytosolic + membrane proteins) which was then subjected to centrifugation at 100,000g for 35 min to obtain membrane protein pellets. Membrane pellets were resuspended in the buffer containing 50 mM HEPEPS-KOH (pH 7.5), 10% glycerol, 2 mM EGTA, 2 mM EDTA, 1 mM DTT, 1 mM PMSF, and protease inhibitor cocktail. After quantification of membrane proteins, the samples were subjected to SDS-PAGE, transferred onto a nitro-cellulose membrane (GE Lifesciences) and probed with 1/500-diluted anti-GFP rabbit IgG antibody (MBL, cat. # 598) and 1/3,000-diluted horse radish peroxidase (HRP, Abcam [cat. # ab6702]). Chemiluminescence detection was as described above.

Protoplast preparation

Protoplasts were prepared as described previously (Yoo et al., 2007). Arabidopsis leaves from aseptically cultivated 3-week-old plants were cut into 0.5–1 mm strips without petioles and mid-ribs, and incubated in protoplasting enzyme solution (1% cellulose R10, 0.5% macerozyme R10, 0.45 M mannitol, 20 mM MES pH 5.7, and 20 mM KCl) on a shaking incubator (5 rpm) in darkness at 25°C for 14–16 h. The mixture was then combined with an equal volume of W5 solution (2 mM MES pH 5.7, 154 mM NaCl, 125 mM CaCl₂, and 5 mM KCl) before filtering of protoplasts using a 75 μm nylon mesh. Protoplasts were centrifuged at 100g for 1–2 min in a round-bottomed tube. After supernatant removal, the protoplast pellet was incubated on ice for 30 min and then resuspended in MMG solution (4 mM MES pH 5.7 containing 0.5 M mannitol and 20 mM KCl) at room temperature. For PEG-mediated transfection, *Pro35S:CPK29:RFP* plasmid (20 μg) was gently mixed with protoplasts (100 μL) in 110 μL PEG solution (30% PEG4000 in ddH₂O containing 0.2 M mannitol and 100 mM CaCl₂) and incubated at room temperature for 10 min. Next, 400 μL W5 solution was added, and the mixture was gently rocked before centrifugation at 100g for 2 min. After supernatant removal, protoplasts were resuspended in 1 mL WI solution (4 mM MES pH 5.7 containing 0.5 M mannitol and 20 mM KCl) and incubated at room temperature for 4 h. Fluorescence from RFP was observed using a confocal microscope (LSM700, Carl Zeiss).

Confocal microscopy of fluorescent proteins

Observation of fluorescence reporters using a confocal microscope (LSM700, Carl Zeiss) was conducted as described previously (Ganguly et al., 2010). To observe the cytological effects of BFA, seedlings were pretreated with CHX (50 μM) for 30 min and then treated with BFA (concentrations as indicated in corresponding figures) and CHX (50 μM) for variable time periods according to the experiment. For BFA wash-out, the BFA solution was replaced by and then incubated in 0.5 × MS medium. BFA was dissolved in dimethyl sulfoxide (DMSO, 0.05%), and controls included an equivalent amount of DMSO. Quantification of fluorescence signals was performed using ImageJ software.

FRET-FLIM analysis

FRET-FLIM analysis was used to observe the *in vivo* interaction between CPK29 and PIN2. Four-day-old seedlings of the double transgenic line containing both *ProPIN2:PIN2:GFP* and *Pro35S:CPK29:RFP*, which was generated by crossing the two lines, were observed for the FRET-FLIM analysis. Fluorescence confocal imaging and fluorescence lifetime imaging for the analysis were conducted using a scanning confocal microscope SP8 FALCON (Leica Microsystems) with a 40 × objective lens. Picosecond pulsed laser lines (488 and 594 nm) from a white light laser system were used as excitation sources. Two-hybrid photon detectors (HyD1 & HyD3) were used to collect emissions in the ranges of 495–580 nm and 600–770 nm from the root samples, respectively. Fluorescence confocal and lifetime images consisted of 512 × 512 pixels were simultaneously recorded using a galvo-stage and time-correlated single-photon counting technique. During the imaging, the pinhole was set to 1.0. All data manipulations were performed and fitted using the Leica suited software (LAS X Ver.3.5.2). Average lifetime values were calculated by the amplitude-weighted method, and the region of interest (ROI) was set as a rectangle in the root epidermal cell.

FRAP analysis

FRAP analysis was performed as previously described (Ganguly et al., 2014) with modifications. Five-day-old *ProPIN2:PIN2:GFP* seedlings were mounted on a sliding glass with 0.5 × MS medium and 0.1% agarose, and imaged using an LSM700 confocal microscope. For photobleaching, 4-μm wide ROIs were selected at the apical or lateral PM side of the root epidermal cell and bleached with 50 iterations of 488 nm set at 100% transmission. Fluorescence recovery was recorded for 10 min after bleaching with a 1-min interval between frames. FRAP data were normalized using the following equation: $I_n = [(I_t - I_{min}) / (I_{max} - I_{min})] \times 100$, where I_n is the normalized intensity, I_t is the intensity at any time t , I_{min} is the minimum post-photobleaching intensity, and I_{max} is the mean pre-photobleaching intensity (Kleine-Vehn et al., 2011). Fluorescence signal intensity was analyzed with ImageJ software.

RNA isolation and reverse transcription-quantitative PCR analysis

Total RNA was isolated from 9-day-old seedlings using an RNeasy Plant Mini Kit (Qiagen). cDNA was synthesized as described previously (Lee and Cho, 2006). Reverse transcription (RT)-qPCR analyses were performed using amfSure qGreen Q-PCR Master mix (Applied GenDEOT) and a CFX Connect Real-Time PCR Detection System (Bio-Rad). Gene-specific signals were normalized to the *ACTIN2* transcript level. Three independent RNA extractions were made from each sample, and three technical replicate RT-qPCR reactions were performed for each RNA sample. Primers used for quantitation are listed in Supplemental Table S4.

Observation of biological parameters

Emerged LR and LR primordia were observed in 9-day-old seedlings. The number of LRs was equivalent to the number of emerged LRs. LR density was estimated by dividing the emerged LR number by the primary root length in cm. LR primordia were observed after roots were cleared as previously described (Lee et al., 2020). Hypocotyl gravitropism was observed with dark-grown seedlings. Hypocotyl images were taken in the indicated time intervals after 90° gravistimulation, and the bending angle was recorded. Phyllotactic analysis was done by measuring the phyllotactic angles of vegetative leaves from 24-day-old plants. The angle formed by two consecutive leaf axes was estimated using ImageJ software.

Statistical analyses

Statistically significant differences are denoted with different letters (one-way ANOVA with Tukey's unequal N HSD post hoc test, $P < 0.05$; Supplemental Data Set 2) or with asterisks (Student's *t* test as indicated in figures).

Accession numbers

Sequence data and mutant information are in the Arabidopsis Genome Initiative databases under the following accession numbers: AT1G76040 (CPK29), AT1G73590 (*PIN1*), AT5G57090 (*PIN2*), AT1G70940 (*PIN3*), AT2G34650 (*PID*), AT3G187800 (*ACTIN2*), AT5G26930 (*GATA23*), AT2G42430 (*LBD16*), AT2G45420 (*LBD18*), AT3G58190 (*LBD29*), AT5G06080 (*LBD33*), AT1G77690 (*LAX3*), AT2G36010 (*E2Fa*), AT5G14650 (*PG*), AT5G56320 (*EXPA14*), SALK_114657 (*cpk29-1*), and CS347204 (*cpk29-2*).

Supplemental data

The following materials are available in the online version of this article.

Supplemental Figure S1. Effect of Ca^{2+} on *in vitro* phosphorylation of WT and autophosphorylation site-mutated (S446A) CPK29.

Supplemental Figure S2. Schematic domain structure of the CPK29 protein and the characterization of T-DNA insertion mutants of the CPK29 gene.

Supplemental Figure S3. Alignments of amino acid sequences of the PINs-HL part from PIN homologs.

Supplemental Figure S4. CPK29-mediated phosphorylation sites of PINs-HL and CPK29.

Supplemental Figure S5. Conservation of S446 among close CPK29 homologs.

Supplemental Figure S6. Expression patterns of CPK29.

Supplemental Figure S7. CPK29 stably localizes to the PM and co-localizes with PIN2.

Supplemental Figure S8. CPK29-target residue in PIN2 is necessary for normal intracellular trafficking of PIN2.

Supplemental Figure S9. Phosphorylation of CPK29-target residues in PINs facilitates PIN recycling to the PM.

Supplemental Figure S10. Phosphorylation of the CPK29-target site in PIN2-HL facilitates PIN2 trafficking to the lateral PM.

Supplemental Figure S11. Phosphorylation sites on PIN-HL.
Supplemental Table S1. Identification of the phosphorylation sites of CPK29 and PINs by using the mass spectrometry analysis after *in vitro* phosphorylation reaction of PIN-HLs with CPK29.

Supplemental Table S2. Identification of the *in vivo* phosphorylation sites of CPK29 and PINs by using the mass spectrometry analysis from Arabidopsis total proteins.

Supplemental Table S3. Identification of the phosphorylation sites of CPK29 and PINs by using the mass spectrometry analysis after *in vitro* phosphorylation reaction of PIN-HLs with S446A-mutated mCPK29.

Supplemental Table S4. List of primers.

Supplemental Data set S1. Text file of the alignment used for the phylogenetic analysis shown in Supplemental Figure S5A.

Supplemental Data set S2. Statistical analyses.

Acknowledgments

We thank Dr Dolf Weijers for kind provision of the *pGreenIIIM DR5v2::ntdTomato/DR5::n3GFP* vector. LC-MS/MS analysis was carried out by the Core Proteomics Facility in the Department of Biological Sciences at Seoul National University, which is supported by the Center for RNA Research, Institute of Basic Science.

Funding

This research was supported by grants from the National Research Foundation (NRF-2017R1E1A1A01075264). H.L. was partially supported by the Stadelmann–Lee Scholarship Fund, Seoul National University.

Conflict of interest statement. Authors declare no conflict of interest.

References

- Al-Momani S, Qi D, Ren Z, Jones AR (2018) Comparative qualitative phosphoproteomics analysis identifies shared phosphorylation motifs and associated biological processes in evolutionary divergent plants. *J Proteomics* **181**: 152–159
- Armengot L, Marques-Bueno MM, Jaillais Y (2016) Regulation of polar auxin transport by protein and lipid kinases. *J Exp Bot* **67**: 4015–4037
- Barbosa ICR, Hammes UZ, Schwechheimer C (2018) Activation and polarity control of PIN-FORMED auxin transporters by phosphorylation. *Trends Plant Sci* **23**: 523–538
- Barbosa ICR, Zourelidou M, Willige BC, Weller B, Schwechheimer C (2014) D6 PROTEIN KINASE activates auxin transport-dependent growth and PIN-FORMED phosphorylation at the plasma membrane. *Dev Cell* **29**: 674–685
- Benjamins R, Ampudia CS, Hooykaas PJ, Offringa R (2003) PINOID-mediated signaling involves calcium-binding proteins. *Plant Physiol* **132**: 1623–1630
- Benková E, Michniewicz M, Sauer M, Teichmann T, Seifertová D, Jürgens G, Friml J (2003) Local, efflux-dependent auxin gradients as a common module for plant organ formation. *Cell* **115**: 591–602
- Brady SM, Orlando DA, Lee JY, Wang JY, Koch J, Dinneny JR, Mace D, Ohler U, Benfey PN (2007) A high-resolution root

- spatiotemporal map reveals dominant expression patterns. *Science* **318**: 801–806
- Brandt B, Brodsky DE, Xue S, Negi J, Iba K, Kangasjärvi J, Ghassemian M, Stephan AB, Hu H, Schroeder JI** (2012) Reconstitution of abscisic acid activation of SLAC1 anion channel by CPK6 and OST1 kinases and branched ABI1 PP2C phosphatase action. *Proc Natl Acad Sci USA* **109**: 10593–10598
- Chen YH, Kao CH** (2012) Calcium is involved in nitric oxide- and auxin-induced lateral root formation in rice. *Protoplasma* **249**: 187–195
- Cho H-T, Cosgrove DJ** (2002) Regulation of root hair initiation and expansin gene expression in *Arabidopsis*. *Plant Cell* **14**: 3237–3253
- Cho M, Lee SH, Cho H-T** (2007) P-Glycoprotein4 displays auxin efflux transporter-like action in *Arabidopsis* root hair cells and tobacco cells. *Plant Cell* **19**: 3930–3943
- Cho M, Lee ZW, Cho H-T** (2012) ATP-binding cassette B4, an auxin-efflux transporter, stably associates with the plasma membrane and shows distinctive intracellular trafficking from that of PIN-FORMED proteins. *Plant Physiol* **159**: 642–654
- Curran A, Chang IF, Chang CL, Garg S, Milla MA, Barron YD, Li Y, Romanowsky S, Cushman JC, Gribskov M et al.** (2011) Calcium-dependent protein kinases from *Arabidopsis* show substrate specificity differences in an analysis of 103 substrates. *Front Plant Sci* **2**: 36
- Dela Fuente RK, Leopold AC** (1973) A role for calcium in auxin transport. *Plant Physiol* **51**: 845–847
- Delormel TY, Boudsocq M** (2019) Properties and functions of calcium-dependent protein kinases and their relatives in *Arabidopsis thaliana*. *New Phytol* **224**: 585–604
- Dettmer J, Hong-Hermesdorf A, Stierhof Y-D, Schumacher K.** (2006) Vacuolar H⁺-ATPase activity is required for endocytic and secretory trafficking in *Arabidopsis*. *Plant Cell* **18**: 715–730
- Dhonukshe P, Huang F, Galvan-Ampudia CS, Mähönen AP, Kleine-Vehn J, Xu J, Quint A, Prasad K, Friml J, Scheres B** (2010) Plasma membrane-bound AGC3 kinases phosphorylate PIN auxin carriers at TPRXS(N/S) motifs to direct apical PIN recycling. *Development* **137**: 3245–3255
- Di Giorgio JAP, Bienert GP, Ayub ND, Yaneff A, Barberini ML, Mecchia MA, Amodeo G, Soto GC, Muschietti JP** (2016) Pollen-specific aquaporins NIP4;1 and NIP4;2 are required for pollen development and pollination in *Arabidopsis thaliana*. *Plant Cell* **28**: 1053–1077
- Ding Z, Galván-Ampudia CS, Demarsy E, Łangowski Ł, Kleine-Vehn J, Fan Y, Morita MT, Tasaka M, Fankhauser C, Offringa R, et al.** (2011) Light-mediated polarization of the PIN3 auxin transporter for the phototropic response in *Arabidopsis*. *Nat Cell Biol* **13**: 447–452
- Dodd AN, Kudla J, Sanders D** (2010) The language of calcium signaling. *Annu Rev Plant Biol* **61**: 593–620
- Du Y, Scheres B** (2018) Lateral root formation and the multiple roles of auxin. *J Exp Bot* **69**: 155–167
- Friml J, Wisniewska J, Benková E, Mendgen K, Palme K** (2002) Lateral relocation of auxin efflux regulator PIN3 mediates tropism in *Arabidopsis*. *Nature* **415**: 806–809
- Ganguly A, Lee SH, Cho H-T** (2012) Functional identification of the phosphorylation sites of *Arabidopsis* PIN-FORMED3 for its subcellular localization and biological role. *Plant J* **71**: 810–823
- Ganguly A, Lee SH, Cho M, Lee OR, Yoo H, Cho H-T** (2010) Differential auxin-transporting activities of PIN-FORMED proteins in *Arabidopsis* root hair cells. *Plant Physiol* **153**: 1046–1061
- Ganguly A, Park M, Kesawat MS, Cho H-T** (2014) Functional analysis of the hydrophilic loop in intracellular trafficking of *Arabidopsis* PIN-FORMED proteins. *Plant Cell* **26**: 1576–1585
- Ganguly A, Sasayama D, Cho H-T** (2012) Regulation of the polarity of protein trafficking by phosphorylation. *Mol Cells* **33**: 423–430
- Geiger D, Scherzer S, Mumm P, Marten I, Ache P, Matschi S, Liese A, Wellmann C, Al-Rasheid KA, Grill E, et al.** (2010) Guard cell anion channel SLAC1 is regulated by CDPK protein kinases with distinct Ca²⁺ affinities. *Proc Natl Acad Sci USA* **107**: 8023–8028
- Geldner N, Friml J, Stierhof Y-D, Jürgens G, Palme K** (2001) Auxin transport inhibitors block PIN1 cycling and vesicle trafficking. *Nature* **413**: 425–428
- Giacometti S, Marrano CA, Bonza MC, Luoni L, Limonta M, De Michelis MI** (2012) Phosphorylation of serine residues in the N-terminus modulates the activity of ACA8, a plasma membrane Ca²⁺-ATPase of *Arabidopsis thaliana*. *J Exp Bot* **63**: 1215–1224
- Grebe M, Xu J, Möbius W, Ueda T, Nakano A, Geuze HJ, Rook MB, Scheres B** (2003) *Arabidopsis* sterol endocytosis involves actin-mediated trafficking via ARA6-positive early endosomes. *Curr Biol* **13**: 1378–1387
- Haga K, Frank L, Kimura T, Schwechheimer C, Sakai T** (2018) Roles of AGCVIII kinases in the hypocotyl phototropism of *Arabidopsis* seedlings. *Plant Cell Physiol* **59**: 1060–1071
- Hammes U, Murphy AS, Schwechheimer C** (2021) Auxin transporters - a biochemical view. *Cold Spring Harb Perspect Biol* doi: 10.1101/cshperspect.a039875
- Huang F, Zago MK, Abas L, van Marion A, Galvan-Ampudia CS, Offringa R** (2010) Phosphorylation of conserved PIN motifs directs *Arabidopsis* PIN1 polarity and auxin transport. *Plant Cell* **22**: 1129–1142
- Ito T, Ishida S, Oe S, Fukazawa J, Takahashi Y** (2017) Autophosphorylation affects substrate-binding affinity of tobacco Ca²⁺-dependent protein kinase1. *Plant Physiol* **174**: 2457–2468
- Ki D, Sasayama D, Cho H-T** (2016) The M3 phosphorylation site is required for trafficking and biological roles of PIN-FORMED1, 2, and 7 in *Arabidopsis*. *Front Plant Sci* **7**: 1479
- Kim DW, Lee SH, Choi S-B, Won S-K, Heo Y-K, Cho M, Park Y-I, Cho H-T** (2006) Functional conservation of a root hair cell-specific cis-element in angiosperms with different root hair distribution patterns. *Plant Cell* **18**: 2958–2970
- Kleine-Vehn J, Ding Z, Jones AR, Tasaka M, Morita MT, Friml J** (2010) Gravity-induced PIN transcytosis for polarization of auxin fluxes in gravity-sensing root cells. *Proc Natl Acad Sci USA* **107**: 22344–22349
- Kleine-Vehn J, Friml J** (2008) Polar targeting and endocytic recycling in auxin-dependent plant development. *Annu Rev Cell Dev Biol* **24**: 447–473
- Kleine-Vehn J, Leitner J, Zwiewka M, Sauer M, Abas L, Luschnig C, Friml J** (2008) Differential degradation of PIN2 auxin efflux carrier by retromer-dependent vacuolar targeting. *Proc Natl Acad Sci USA* **105**: 17812–17817
- Kleine-Vehn J, Wabnik K, Martiniere A, Langowski L, Willig K, Naramoto S, Leitner J, Tanaka H, Jakobs S, Robert S, et al.** (2011) Recycling, clustering, and endocytosis jointly maintain PIN auxin carrier polarity at the plasma membrane. *Mol Syst Biol* **7**: 540
- Křeček P, Skůpa P, Libus J, Naramoto S, Tejos R, Friml J** (2009) The PIN-FORMED (PIN) protein family of auxin transporters. *Genome Biol* **10**: 249
- Łangowski Ł, Wabnik K, Li H, Vanneste S, Naramoto S, Tanaka H, Friml J** (2016) Cellular mechanisms for cargo delivery and polarity maintenance at different polar domains in plant cells. *Cell Discovery* **2**: 16018
- Latz A, Mehler N, Zapf S, Mueller TD, Wurzing B, Pfister B, Csaszar E, Hedrich R, Teige M, Becker D** (2013) Salt stress triggers phosphorylation of the *Arabidopsis* vacuolar K⁺ channel TPK1 by calcium-dependent protein kinases (CDPKs). *Mol Plant* **6**: 1274–1289
- Lee H, Ganguly A, Lee RD, Park M, Cho H-T** (2020) Intracellularly localized PIN-FORMED8 promotes lateral root emergence in *Arabidopsis*. *Front Plant Sci* **10**: 1808
- Lee OR, Kim SJ, Kim HJ, Hong JK, Ryu SB, Lee SH, Ganguly A, Cho H-T** (2010) Phospholipase A2 is required for PIN-FORMED protein

- trafficking to the plasma membrane in the *Arabidopsis* root. *Plant Cell* **22**: 1812–1825
- Lee SH, Cho H-T** (2006) PINOID positively regulates auxin efflux in *Arabidopsis* root hair cells and tobacco cells. *Plant Cell* **18**: 1604–1616
- Leitner J, Petrásek J, Tomanov K, Retzer K, Parezová M, Korbei B, Bachmair A, Zazimalová E, Luschnig C** (2012) Lysine63-linked ubiquitylation of PIN2 auxin carrier protein governs hormonally controlled adaptation of *Arabidopsis* root growth. *Proc Natl Acad Sci USA* **109**: 8322–8327
- Liao C-Y, Smet W, Brunoud G, Yoshida S, Vernoux T, Weijers D** (2015) Reporters for sensitive and quantitative measurement of auxin response. *Nat Methods* **12**: 207–210
- Maierhofer T, Diekmann M, Offenborn JN, Lind C, Bauer H, Hashimoto K, Alrasheid KAS, Luan S, Kudla J, Geiger D, et al.** (2014) Site- and kinase-specific phosphorylation-mediated activation of SLAC1, a guard cell anion channel stimulated by abscisic acid. *Science Signaling* **7**: ra86
- Menz J, Li Z, Schulze WX, Ludewig U** (2016) Early nitrogen-deprivation responses in *Arabidopsis* roots reveal distinct differences on transcriptome and (phospho-) proteome levels between nitrate and ammonium nutrition. *Plant J* **88**: 717–734
- Mergner J, Frejno M, List M, Papacek M, Chen X, Chaudhary A, Samaras P, Richter S, Shikata H, Messerer M, et al.** (2020) Mass-spectrometry-based draft of the *Arabidopsis* proteome. *Nature* **579**: 409–414
- Ötvös K, Marconi M, Vega A, B'Brien J, Johnson A, Abualia R, Antonielli L, Montesinos JC, Zhang Y, Tan S, et al.** (2021) Modulation of plant root growth by nitrogen source-defined regulation of polar auxin transport. *EMBO J* **40**: e106862
- Popescu SC, Popescu GV, Bachan S, Zhang Z, Seay M, Gerstein M, Snyder M, Dinesh-Kumar SP** (2007) Differential binding of calmodulin-related proteins to their targets revealed through high-density *Arabidopsis* protein microarrays. *Proc Natl Acad Sci USA* **104**: 4730–4735
- Qi B, Zheng H.** (2013) Modulation of root-skewing responses by KNAT1 in *Arabidopsis thaliana*. *Plant J* **76**: 380–392
- Rakusová H, Gallego-Bartolomé J, Vanstraelen M, Robert HS, Alabadi D, Blázquez MA, Benková E, Friml J** (2011) Polarization of PIN3-dependent auxin transport for hypocotyl gravitropic response in *Arabidopsis thaliana*. *Plant J* **67**: 817–826
- Reyes FC, Buono R, Otegui MS** (2011) Plant endosomal trafficking pathways. *Curr Opin Plant Biol* **14**: 666–673
- Rigó G, Ayaydin F, Tietz O, Zsigmond L, Kovács H, Páy A, Salchert K, Darula Z, Medzihradzky KF, Szabados L, et al.** (2013) Inactivation of plasma membrane-localized CDPK-RELATED KINASE5 decelerates PIN2 exocytosis and root gravitropic response in *Arabidopsis*. *Plant Cell* **25**: 1592–1608
- Ronzier E, Corratgé-Faillie C, Sanchez F, Prado K, Brière C, Leonhardt N, Thibaud J-B, Xiong TC** (2014) CPK13, a noncanonical Ca^{2+} -dependent protein kinase, specifically inhibits KAT2 and KAT1 shaker K^+ channels and reduces stomatal opening. *Plant Physiol* **166**: 314–326
- Saha P, Singh M** (1995) Characterization of a winged bean (*Psophocarpus tetragonolobus*) protein kinase with calmodulin-like domain: regulation by autophosphorylation. *Biochem J* **305**: 205–210
- Sasayama D, Ganguly A, Park M, Cho H-T** (2013) The M3 phosphorylation motif has been functionally conserved for intracellular trafficking of long-looped PIN-FORMEDs in the *Arabidopsis* root hair cell. *BMC Plant Biol* **13**: 189
- Schulz P, Piepenburg K, Lintermann R, Herde M, Schöttler MA, Schmidt LK, Ruf S, Kudla J, Romeis R, Bock R** (2021) Improving plant drought tolerance and growth under water limitation through combinatorial engineering of signalling networks. *Plant Biotech J* **19**: 74–86
- Toyota M, Furuichi T, Tatsumi H, Sokabe M** (2008) Cytoplasmic calcium increases in response to changes in the gravity vector in hypocotyls and petioles of *Arabidopsis* seedlings. *Plant Physiol* **146**: 505–514
- Valmonte GR, Arthur K, Higgins CM, MacDiarmid RM** (2014) Calcium-dependent protein kinases in plants: evolution, expression and function. *Plant Cell Physiol* **55**: 551–569
- Wang X, Bian Y, Cheng K, Gu LF, Ye M, Zou H, Sun SS-M, He J-X** (2013) A large-scale protein phosphorylation analysis reveals novel phosphorylation motifs and phosphoregulatory networks in *Arabidopsis*. *J Proteomics* **14**: 486–498
- Wang Y, Liang S, Xie QG, Lu YT** (2004) Characterization of a calmodulin-regulated Ca^{2+} -dependent-protein-kinase-related protein kinase, AtCRK1, from *Arabidopsis*. *Biochem J* **383**: 73–81
- Weller B, Zourelidou M, Frank L, Barbosa ICR, Fastner A, Richter S, Jürgens G, Hammes UZ, Schwechheimer C** (2017) Dynamic PIN-FORMED auxin efflux carrier phosphorylation at the plasma membrane controls auxin efflux-dependent growth. *Proc Natl Acad Sci USA* **114**: E887–E896
- Wiśniewska J, Xu J, Seifertová D, Brewer PB, Růžicka K, Blilou I, Rouquié D, Benková E, Scheres E, Friml J** (2006) Polar PIN localization directs auxin flow in plants. *Science* **312**: 883–883
- Xu J, Scheres B** (2006) Polar auxin transport and patterning: grow with the flow. *Genes Dev* **20**: 922–926
- Yang Z, Guo G, Zhang M, Liu CY, Hu Q, Lam H, Cheng H, Xue Y, Li J, Li N** (2013) Stable isotope metabolic labeling based quantitative phosphoproteomic analysis of *Arabidopsis* mutants reveals ethylene-regulated time-dependent phosphoproteins and putative substrates of constitutive triple response 1 kinase. *Mol Cell Proteomics* **12**: 3559–3582
- Yoo S-D, Cho Y-H, Sheen J** (2007) *Arabidopsis* mesophyll protoplasts: a versatile cell system for transient gene expression analysis. *Nat Protocol* **2**: 1565–1572
- Zhang J, Vanneste S, Brewer PB, Michniewicz M, Grones P, Kleine-Vehn J, Löffke C, Teichmann T, Bielach A, Cnannot B, et al.** (2011) Inositol trisphosphate-induced Ca^{2+} signaling modulates auxin transport and PIN polarity. *Dev Cell* **20**: 855–866
- Zourelidou M, Müller I, Willige BC, Nill C, Jikumaru Y, Li H, Schwechheimer C** (2009) The polarly localized D6 PROTEIN KINASE is required for efficient auxin transport in *Arabidopsis thaliana*. *Development* **136**: 627–636
- Zourelidou M, Absmanner B, Weller B, Barbosa ICR, Willige BC, Fastner A, Streit V, Port SA, Colcombet J, de la Fuente van Bentem S, et al.** (2014) Auxin efflux by PIN-FORMED proteins is activated by two different protein kinases, D6 PROTEIN KINASE and PINOID. *eLife* **3**: e02860